LAWRENCE
LIVERMORE
NATIONAL
LABORATORY

LLNL-JRNL-665817

Characterizing the Plasmas of Z-Pinches (Mini-Tutorial)

D. D. Ryutov

January 6, 2015

IEEE Transactions on Plasma Science

Disclaimer

LLNL-JRNL-665817

Characterizing the Plasmas of Z-Pinches

(Mini-Tutorial)

D.D. Ryutov

Lawrence Livermore National Laboratory, Livermore, CA 94550

Abstract. This article summarizes the plasma characteristics important for the Z-pinch research. It begins with the discussion of the most basic plasma properties related to collisionality and magnetization and then proceeds to more complex phenomena associated with magnetic field evolution in a highly dynamical plasma. Plasma transport properties are discussed mostly in conjunction with the MagLIF concept. Issues of interplay of the classical and anomalous transport in a plasma whose pressure is higher than the magnetic pressure are elucidated. Differences between the magnetic reconnection in a weakly and highly-collisional plasmas are discussed. Kinetic effects and the role of microturbulence are mentioned in conjunction with formation of high-energy tails in the particle distribution functions and generation of particle beams. Discussion is based on the order-of-magnitude estimates suitable for initial orientation in the problem. A set of numerical relations that can be used for quick estimates is presented in Appendix.

1. INTRODUCTION

The plasmas of Z-pinches occupy a very large domain in a parameter space. Their common feature is a high plasma pressure p that can be much higher than the magnetic pressure p_M; another important feature of these plasmas is that the magnetic field is entirely or almost entirely created by the currents flowing in the plasma itself, unlike the magnetic confinement systems - tokamaks, stellarators, or mirrors. Together, this creates an environment of incredibly dynamic, rapidly evolving systems, sometimes showing the trend to fractalization.

In a number of situations, this plasma is so dense that it is strongly collisional and can therefore be reasonably well described by the two-fluid model and, sometimes, even by an additionally reduced model of resistive single-fluid magnetohydrodynamic (MHD). However, even in these situations of an apparent strong collisionality, the rapidly evolving plasma of Z-pinches is prone to the effects of magnetic reconnection and current disruptions that may trigger the processes of particle acceleration, both in the form of the particle beams and in the form of long quasi-isotropic "tails" of the distribution functions. In other cases, the whole plasma may become hot and weakly collisional.

This tutorial represents a theorist's view on the most salient features of the Z-pinch plasmas. The author attempts to identify the dominant effects and the ways of their description most suitable for various specific settings. We start from very basic assessment of the simplest plasma characteristics of collisionality and magnetization and move on to describe more complex effects depending on these two basic characteristics. This tutorial will allow the reader to approximately locate the position of his/her plasma in a multi-dimensional parameter space and qualitatively identify effects that are of the most importance in this plasma. It will also present a concept of scalability and illustrate how the scaling relations between various laboratory experiments, as well as between the astrophysical and laboratory plasmas can be established.

This tutorial does not cover techniques used to produce Z-pinches and some other configurations closely related to Z-pinches. Figure 1 is provided simply to illustrate the general shape of these objects (see also bibliographic references at the end of this section). The basic "classical" Z-pinch is shown in Fig. 1a. The strong axial ("z") current creates a compression force acting on the cylindrical liner. In the dynamical systems the current grows rapidly, and accelerates the liner towards the axis where it collapses, creating a very dense and hot object that quickly rebounds. There is also a different possibility, where the plasma is created in a quasistatic equilibrium, with the radial plasma pressure gradient balanced by the $\boldsymbol{j} \times \boldsymbol{B}$ force (the so called "Bennett pinch"). Both configurations are unstable. In the equilibrium case the instability is related to the increase (decrease) of the azimuthal magnetic field in the zone of decreased (increased) radius of the current column. This factor affects stability of imploding plasmas as well, but in this latter case it is usually subdominant relative to to the Rayleigh-Taylor instability driven by the effective gravity force directed against the density gradient. As this acceleration-driven instability is caused by the magnetic forces, it is sometimes called "Magnetic Rayleigh-Taylor" instability (MRT).

Besides "canonical" pinch configuration shown in Fig. 1a there exist other configurations that share many pieces of the basic physics with the "canonical" one but look sometimes quite differently. In particular, the plasma focus (Fig. 1b) is characterized by the formation of a discharge channel (plasma shell) between two coaxial cylindrical electrodes early in the pulse; the $\boldsymbol{j} \times \boldsymbol{B}$ force causes a gradual acceleration of this plasma along the annulus, curving of the shell, and its eventual implosion in a manner reminiscent of that sown in Fig. 1a.

Very high current densities can be reached in the x-pinches (Fig. 1c), where the discharge occurs in the X-shaped intersection of two or more thin wires (or in the neck of a specially machined conical conductors).

The mutual attraction of the currents that causes the pinch implosion in Fig. 1a occurs also if there is no axial symmetry in the current pattern. This is realized in the linear arrays of current-carrying wires.

It is impossible to cover enormous literature related to the Z-pinches and Z-pinch plasmas in this relatively compact tutorial – a complete list of references would be a few times longer than this whole article! So, the author has to be quite selective in this regard and has limited himself to a small sub-set of references. Still, the references cited in this article will allow the reader to orient himself/herself in the relevant issues and also find further references in the cited papers.

To guide those readers who are only interested in a quick orientation in te achievements in this research area, the author provides here an even smaller subset of references with brief explanations. Summary of the early research on Z pinches can be found in Ref. 1. Broad reviews of Z pinches are presented in Refs. 2, 3. Applications of Z pinches as radiation sources are described in Ref. 4. A lot of information on the wire-array Z-pinches is provided in Ref. 5, whereas experiments on linear wire arrays are described in Ref. 6. The X-pinches are discussed in Ref. 7 and their use as point X-ray sources, in Ref. 8. Recent analyses of the plasma foci are presented in Ref. 9. Scaling relations between various experiments are provided in Ref. 10, whereas scaling relations between phenomena in distant astrophysical objects and laboratory plasmas, in Refs. 11, 12. The fusion applications include a MagLIF concept [13] that is based on a rapid adiabatic compression of a cylindrical plasma with a pre-imposed axial magnetic field, and Magnetized Target Fusion [MTF] approach (e.g., [14, 15]) that involves compression of the closed-field-line configuration (e.g., the Field-Reversed Configuration, FRC) by a somewhat

slower implosions. We do not discuss the studies on the MHD stability of Z pinches – this would require at least one more tutorial. The representative references, aside from the reviews [2, 3], are Refs. [16, 17]. As a main source of information on plasma transport we use a fundamental review by S. I. Braginski [18]. As already mentioned, more references will be provided in the subsequent sections.

Throughout the paper we use CGS units. In "practical" numerical estimates mixed units are used, specified in each case.

2. GENERAL CHARACTERIZATION OF THE Z-PINCH PLASMAS

2.1 Collisionality

We start this section from presenting convenient estimates for the electron and ion mean-free paths (mfp):

$$\lambda_{ei}(cm) \approx \frac{2\cdot 10^{18}\left[T_e(keV)\right]^2}{Zn_e(cm^{-3})};\ \lambda_{ii}(cm) \approx \frac{2\cdot 10^{18}\left[T_e(keV)\right]^2}{Z^3 n_e(cm^{-3})}\ . \qquad (1)$$

Here n_e is the electron density, $T_{e,i}$ are the particle temperatures, and Z is an average charge state of the ions. The estimates are based on equations presented in review [18]. One can note that the particle mean-free-path in a plasma depends on the particle energy, and an "exact" value of λ depends on the averaging procedure that is different for the evaluation of different transport coefficients, say, thermal conductivity and plasma resistivity. Therefore, Eq. (1) can be considered as a *definition* of the mfp for the thermal particles. If the plasma is grossly non-Maxwellian, the collisions depend on the position of the particle in question in the velocity space and have to be described by a full-blown collision operator [19]. The numerical factors in Eq. (1) are chosen so as to provide a sense of the scales determining such processes as the electron scattering on ions, or isotropization of the initially anisotropic ion distribution. The Coulomb logarithm is chosen to be about 10, a reasonable estimate for the Z-pinch plasmas. Equations (1) correspond to thermal particles; for the higher-energy tail of the distribution functions the mean-free path scales as $(E/T)^2$, where $E>>T$ is an energy of the tail particle. A detailed review of collisions in plasmas can be found in Ref. [19].

Here and below we consider "simple" plasmas, with a single ion species of the atomic mass A and charge Z. For the DT plasma we take A=2.5, Z=1. For a partially ionized plasmas, one can approximately identify Z with the average ion charge. Due to the fact that the electron-ion cross-section scales as Z^2, and the ion density is equal to n_e/Z, the electron-ion mean-free-path contains parameter $1/Z$ when expressed in terms of the electron density The ion-ion collision cross-section scales as Z^4 and, accordingly, the ion-ion m.f.p. scales as Z^{-3} at a given n_e. At lower temperatures and higher densities one may enter a regime of a non-ideal plasma, where thermal particle energies would become smaller than the Coulomb interaction energies. This regime corresponds usually to an early stage of the discharge, where the melting and evaporation of the conductor begin [20]. We will not dwell on these issues.

The dimensionless parameter ("collisionality") that would characterize the effect of collisions on the plasma transport over the scale L can be introduced as

$$Col_e = \frac{L}{\lambda_{ei}};\ Col_i = \frac{L}{\lambda_{ii}}\ . \qquad (2)$$

Note that we use an acronym *Col* with more than one letter (*Col* instead of *C*) in order not to confuse collisionality with the radial liner convergence *C* extensively used later in this article. Such notation also follows traditions of the dimensionless analysis, where the extended acronyms have been used for many decades (like *Re* instead of *R* for the Reynolds number).

The parameter directly related to the m.f.p. is the collision time $\tau_{e,i}$ that we define as the electron or ion m.f.p. divided by the thermal velocity of the respective particle, $\mathrm{v}_{Te,i} = \sqrt{2T_{e,i} / m_{e,i}}$:

$$\tau_{e,i} = \lambda_{e,i} / \mathrm{v}_{Te,i} . \qquad (3)$$

The inverse quantity is called the collision frequency, $\nu_{ei} \equiv 1/\tau_{e,i}$.

In the context of pulsed Z-pinch plasmas, the particle mean-free path is significant in several respects. First, it strongly affects the electron behaviour on the open magnetic field lines. Consider first the situation of a large electron m.f.p. $Col_e = L/\lambda_{ei} << 1$, where L is a plasma scale-length along the magnetic flux tube. If the ends of the flux tube are in contact with a cold plasma (e.g., a blow-off plasma of the end electrodes), a very rapid replacement of hot electrons by the cold ones would occur. On the other hand, if the ends are flaring into the empty space, then, in principle, an ambipolar electric field could hold hot electrons and maintain a slow electron loss in the regime "one electron lost per one ion lost," like in the mirror confinement [21]. But this would require the presence of the vacuum volumes at the ends.

Conversely, for a short electron mean-free path, an electron temperature gradient can be sustained along the flux tube, with the heat flux to the ends determined by the electron thermal conductivity. The possibility to describe the electron heat flux in terms of thermal conductivity requires actually pretty large values of the collisionality parameter, as the main contribution to the heat flux comes from the electrons that have energy a few times higher than electron thermal energy [18] and, respectively, significantly larger mean free path than thermal electrons. Therefore, for Col_e <10 one has to use one of the models for heat flux limitation (see brief summaries in Refs. [22, 23]).

Likewise, if the ratio $Col_i = L/\lambda_{ii}$ for DT ions is not sufficiently large, the high energy tails of the ion distribution that are responsible for the fusion reactivity at modest plasma temperatures (T_i<10-15 keV, Ref. 24), would be rapidly depleted through the end loss, that leading to a reduced reactivity. The essence of this problem has been described in Refs. 25-27, and detailed simulations for the ICF setting are published in Ref. 28 where further references are also given.

Yet another effect where the parameter *Col* plays a significant role is the mesoscale plasma turbulence that may drive the anomalous transport (Bohm-like transport), see, e.g., Refs. [29, 30]: this parameter enters an expression for the growth rates of the drift-type perturbations, see Sec. 7.

Table 1 presents the plasma parameters for several regimes characteristic of the Z pinches. They do not correspond to any particular experiment, just indicate a rough range of parameters that can be met: line 1 corresponds to a DT plasma at the initial state of the MagLIF implosion, and line 2 to the final stage of this implosion; Line 3 corresponds to plasmas that can be formed during the fast heating of the wire at the early stage of the wire array implosion; Line 4 describes the plasma that appears in the experiments on the astrophysics-relevant jet formation; Line 5 contains parameters of the plasma that may be formed outside the liner early in the pulse. Parameter L corresponds to a cross-field spatial scale of the plasma

Figure 2 shows the split of the (n_e, T) plane by the lines of a constant m.f.p. These lines represent the parameter $Z\lambda_{ei}$ for the electrons and parameter $Z^3\lambda_{ii}$ for the ions. Note that the

horizontal axis is in the units of the *electron* density. Shown in coloured dots are the locations of several typical plasmas. The red line corresponds to a sequence of states of the core plasma during the MagLIF implosion [13]. This is a hydrogen plasma and, accordingly, Z=1. A blue dot illustrates a plasma of the wire array during the run-in phase of the implosion [31]. We assume that the average charge state corresponds to Z=6. With that, the electron-ion mean-free path is ~40 times longer that the ion-ion mean-free path. The green dot marks a plasma produced in the astrophysics-related jet experiments of the type [32]. Just these three examples show the breadth of the parameter space occupied by the Z-pinch plasmas.

Table 1 Plasma parameters of relevance to Z-pinches

	n_e, cm^{-3}	T_e, eV	Z	A	B, T	$L_\perp$, cm
1	$7.2\cdot10^{20}$	300	1	2.5	30	0.2
2	6×10^{23}	10^4	1	2.5	10^4	0.007
3	10^{23}	25	6	27	300	0.0005
4	10^{19}	25	6	27	30	0.3
5	10^{18}	50	6	12	100	0.1

Another important parameter characterizing the plasma collisionality is the temperature equilibration time between the electrons and the ions. The equilibration time is evaluated according to equation (see Eqs. (2.3) and (2.17) in Ref. 18):

$$\tau_{ei}^{(E)}(ns) = 10^{21}\frac{A\left[T_e(keV)\right]^{3/2}}{Zn_e(cm^{-3})}. \qquad (4)$$

This time is important in the cases where the heating power goes initially into one of the plasma components, electrons or ions. In particular, in the MagLiF setting, the initial laser preheat goes predominantly into the electrons. The equilibration time is important for the electron-ion coupling in the problem of the heat transport. The temperature equilibration affects also the thresholds and growth rates of the ion-acoustic and drift instabilities (see Secs. 7 and 9).

Figure 2 shows the lines of $\tau_{ei}^{(E)} = const$ in the (n, T) plane. For a DT plasma of MagLIF, with A=2.5, Z=1, the energy exchange time early in the implosion is 1-2 ns, which is sufficient to equalise the temperatures before the rapid change of the plasma radius begins. For other elements, the factor A/Z is close to 2.

2.2. Magnetization

We will define the magnetization parameter *Mag* as the product of the electron (ion) collision time and the corresponding cyclotron frequency (also called sometimes "gyrofrequency"), $\omega_{Ce,i} = ZeB / m_{e,i}c$:

$$Mag_{e,i} = \omega_{Ce,i}\tau_{e,i} \tag{5}$$

We again use an acronym with more than one letter (*Mag* instead of *M*), not to confuse magnetization with the Mach number that is mentioned later in this article. Numerically, one has the following expressions for *Mag*:

$$Mag_e \approx 3\cdot 10^{20}\frac{\left[T_e(keV)\right]^{3/2}B(T)}{Zn_e(cm^{-3})};\quad Mag_i \approx 6\cdot 10^{18}\frac{\left[T_i(keV)\right]^{3/2}B(T)}{\sqrt{A}Z^2 n_e(cm^{-3})} \tag{6}$$

If the magnetization parameter is large, a host of the transport phenomena in the corresponding plasma component becomes strongly dependent of the magnetic field and significantly anisotropic. In particular, the electron thermal diffusivity across the magnetic field decreases by a large factor compared to the unmagnetized case (see Sec. 6). As is clear from expressions (6), the strong magnetization of the electrons requires much lower magnetic fields than the magnetization of the ions. So, in a number of cases one may find the situation where the electrons are magnetized, whereas the ions are not. Under the typical conditions of dense Z-pinch plasmas, the electrons are magnetized in hotter areas and un-magnetized in colder ones. The partition of the (*n,T*) plane for the electrons and ions is shown in Fig. 3. The ions are magnetized above the corresponding lines. By locating the characteristic point for a particular experiment in Fig. 3, one can find out which version of the ion transport coefficients has to be used. For the electrons, as mentioned, the magnetized version is typical.

2.3. Plasma beta

The ratio of the plasma pressure *p* to the magnetic pressure p_M is obviously important in determining the plasma equilibria and macroscopic stability, but it also affects a number of other plasma processes, like wave propagation, microinstabilities, and transport phenomena. This (dimensionless) ratio, usually denoted as β, can be written as

$$\beta = 4\times 10^{-16}\frac{n_e(cm^{-3})\left[T_e(keV)+\dfrac{T_i(keV)}{Z}\right]}{\left[B(T)\right]^2} \tag{7}$$

Note that for the plasma with significant ion charge, the plasma pressure at comparable electron and ion temperatures is determined predominantly by the electrons. This has important ramifications for the properties of the shock waves in such plasmas, because the upstream kinetic energy is distributed behind the shock between numerous electrons, this leading to a more modest temperature increase than the one that could be anticipated in the plasma with Z=1.

This large electron contribution to the pressure of the Z>>1 plasma affects the properties of the ion acoustic waves creating a possibility for these waves to be weakly damped even in the plasma with T_e=T_i (unlike the Z=1 plasma where the ion acoustic waves experience a strong Landau damping on the ions, if T_e=T_i), see e.g., Ref. 33. The reason is that the ion acoustic wave propagates at the speed $\sim\sqrt{p/\rho}\sim\sqrt{ZT/Am_p}$, whereas the ion thermal velocity is $\sim\sqrt{T/Am_p}$,

i.e., significantly smaller than the sound speed for Z>>1, thereby making the ion Landau damping small.

The partition of the (n,T) plane by the lines of constant β is shown in Fig. 4 for the case of $T_e=T_i$. It is worthwhile to note that for $\beta\sim1$ in a plasma of singly-charged ions one automatically has the two important spatial scales, the ion gyro-radius ρ_i and the ion collisionless skin-depth, c/ω_{pi} approximately equal to each other. In a more general case of an arbitrary Z,

$$\frac{\rho_i}{c/\omega_{pi}} \approx \sqrt{\frac{\beta}{Z}} \tag{8}$$

3. MAGNETIC FIELD EVOLUTION

3.1 Basic equations

Magnetic field evolution for the processes occurring on the time-scales much longer than the light transit time is described by the quasi-stationary Maxwell equations,

$$\frac{\partial \boldsymbol{B}}{\partial t} = -c\nabla\times\boldsymbol{E};\quad \nabla\times\boldsymbol{B} = \frac{4\pi}{c}\boldsymbol{j}, \tag{9}$$

where the current density is:

$$\boldsymbol{j} = en_e\boldsymbol{u};\quad \boldsymbol{u} \equiv \left(\mathbf{v}-\mathbf{v}_e\right), \tag{10}$$

and the plasma charge neutrality is assumed, $Zn_i=n_e$. In this equation, $\mathbf{v}$ is the ion velocity that is equal to a high accuracy to the plasma hydrodynamic velocity (the electron-to-ion mass ratio is small), whereas $\boldsymbol{u}$ is a relative velocity of the electrons and ions, the "current" velocity. Equation (10) holds both for the plasma of hydrogen isotopes and plasmas with Z>1.

The electron momentum equation [18] relates the electric field to the plasma parameters:

$$0 = -\nabla(n_eT_e) - en_e\left(\boldsymbol{E}+\frac{\mathbf{v}_e\times\boldsymbol{B}}{c}\right) + \boldsymbol{F}_T + \boldsymbol{F}_{ei}. \tag{11}$$

where we neglect the inertial terms on the left-hand side due to smallness of the electron mass; we also neglect the electron viscosity, as it is very small compared to the pressure term. The retained terms in Eq. (11) have the following meaning: the first term is the pressure gradient, the second is the Lorentz force, the third is the electron thermal force (see below), and the last term describes the electron friction against the ions and is proportional to the "current" velocity $\boldsymbol{u}$.

Solving Eq. (11) for $\boldsymbol{E}$, substituting the result into the first of Eqs. (9), and using Eq. (10) to express $\mathbf{v}_e$ in terms of $\boldsymbol{j}$ and $\mathbf{v}$, one finds:

$$\frac{\partial \boldsymbol{B}}{\partial t} = \underbrace{\nabla\times\left[\mathbf{v}\times\boldsymbol{B}\right]}_{\text{"1"}} \underbrace{-\frac{c}{e}\nabla\times\left[\frac{\boldsymbol{j}}{n_e}\times\boldsymbol{B}\right]}_{\text{"2"}} \underbrace{+\frac{c}{e}\nabla\times\frac{\boldsymbol{F}_{ei}}{n_e}}_{\text{"3"}} \underbrace{+\frac{c}{en_e}\left[\nabla n_e\times\nabla T_e\right]}_{\text{"4"}} \underbrace{+\frac{c}{e}\nabla\times\frac{\boldsymbol{F}_T}{n_e}}_{\text{"5"}}. \tag{12}$$

We have numbered the terms in the right-hand-side to identify them more easily in the discussion below.

3.2 Hall effect

The term "1" in Eq. (12) describes the frozen-in effect for the limiting case where the magnetic field is advected by the plasma flow with the plasma *hydrodynamic velocity* $\mathbf{v}$. The

second term is related to the fact that the magnetic field is actually advected with the *electron flow velocity* $\mathbf{v}_e$, as is clear from Eq. (11). This term describes the so-called Hall effect and can be neglected if the current density $\boldsymbol{j}$ is sufficiently small, so that the current velocity $\boldsymbol{u}$ is much smaller than the characteristic hydrodynamic velocity $\mathbf{v}$. For the latter, depending on the nature of the flow, one can take an Alfven velocity v_A or the ion sound velocity c_s. Note that, though the second term becomes zero if $\boldsymbol{j}$ is parallel to $\boldsymbol{B}$, the constraint on the current density is still important, as it affects the evolution of various perturbations, in which the magnetic field may be not aligned with the current flow. The corresponding effects are described by the so called "Electron Magnetohydrodynamics" or "Hall Magnetohydrodynamics" [34]. Given that the current velocity is related to the magnetic field B and the length-scale L by $u = (c/4\pi e n_e)(B/L)$, one can formulate the following condition for the current velocity to be less than the Alfven velocity, $u<v_A$:

$$L > \frac{c}{\omega_{pi}}; \quad \omega_{pi} = \sqrt{\frac{4\pi n_e e^2}{m_p}}\sqrt{\frac{Z}{A}} \ . \tag{13}$$

The role of the Hall effect can be characterized by the dimensionless ratio that we call the "Hall number", Ha, the ratio of u to v_A:

$$Ha \equiv \frac{c}{L\omega_{pi}} . \tag{14}$$

Note that our dimensionless Hall number is different from a Hall parameter used in a solid-state physics (e.g., [35]) and characterizing the voltage across the current-carrying sample immersed into magnetic field perpendicular to the current. The "practical" expression for our Ha reads:

$$Ha \approx \frac{2.3\cdot 10^7}{L(cm)\sqrt{n_e(cm^{-3})}}\sqrt{\frac{A}{Z}} . \tag{15}$$

The partition of the parameter space by the lines of constant Ha for several values of L is shown in Fig. 5. [The multiplier $\sqrt{Z/A}$ makes the plot independent of Z and A.] Large values of Ha mean that the Hall effect is important, and vice versa. The role of Hall effect in the laboratory pulsed-power-based experiments imitating astrophysical jets has been assessed in Ref. 36, 37.

3. 3 Electron-ion friction

The term "3" in Eq. (12) describes resistive diffusion/dissipation of the magnetic field. The electron-ion friction force has two components, parallel to the magnetic field and perpendicular to it. The first does not depend on the magnetization and can be written as $F_{\|ei} = -em_e n_e \nu_{ei} u_\|$. The second is proportional to $u_\perp$, with a coefficient somewhat dependent on the electron magnetization. This dependence is, however, relatively weak: in the case of weak magnetization the coefficient is the same as for the parallel force and in the case of strong magnetization it becomes by approximately factor of 2 higher than in the un-magnetizes case (see [18]). In the spirit of our broad qualitative approach we will neglect this difference and write: $\boldsymbol{F}_{ei} = -em_e n_e \nu_{ei}\boldsymbol{u} = -m_e \nu_{ei}\boldsymbol{j}$. The third term in Eq. (12) then becomes $\nabla\times\left(D_M \nabla\times\boldsymbol{B}\right)$, where D_M is called "the magnetic diffusivity" and is related to the plasma electrical conductivity σ by

$$D_M = c^2 / 4\pi\sigma\,, \tag{16}$$

with $\sigma = \omega_{pe}^2 / 4\pi\nu_{ei}$. For a uniform D_M one has $\nabla\times\left(D_M\nabla\times\boldsymbol{B}\right) = D_M\nabla^2\boldsymbol{B}$, a pure diffusion. We will discuss the relation of this term and the advection term in Section 4.

3.4 Biermann battery and Nernst effect

The last two terms ("4" and "5") in the r.h.s. of Eq. (12) have a distinctly different structure from the first three ones: the terms "1"-"3" turn zero in the absence of the magnetic field, whereas the terms "4"-"5", generally speaking, do not. These latter ones describe generation of the magnetic field and serve as source terms in Eq. (12). If one goes back to Eq. (11) and drops there $\boldsymbol{B}$, one sees that these two terms act as an electromotive force. Of them, the term "4" leads to the magnetic field generation when the temperature and density gradients are not collinear to each other. This is an effect sometimes called (especially in the astrophysical literature) "a Biermann battery effect" [38, 39].

The term "5" has a more complex structure and depends significantly on the magnetization. It is (see Eq. (4.31) in Ref. 18, mind the difference in notation):

$$\boldsymbol{F}_T = n_e\left(-\alpha_{\|}\nabla_{\|}T_e - \alpha_{\perp}\nabla_{\perp}T_e - \alpha_{\wedge}\boldsymbol{b}\times\nabla T_e\right), \tag{17}$$

where $\boldsymbol{b}\equiv\boldsymbol{B}/B$ is a unit vector in the magnetic field direction, and the coefficients $\alpha_{\perp},\alpha_{\wedge}$ depend significantly on the electron magnetization Mag_e. The last term in Eq. (17) describes the component of the force perpendicular to both the magnetic field and the electron temperature gradient ("Nernst effect"). This last term has a structure of the other advective terms, "1" and "2".

For weak magnetic fields, where the magnetization parameter is small ("weak magnetization") an expression for the thermal force, up to the first-order terms in the magnetization parameter, reads as:

$$\boldsymbol{F}_T \approx -0.71 n_e\nabla T_e - \alpha_1 n_e\frac{e\boldsymbol{B}\times\nabla T_e}{m_e c\nu_{ei}}\,, \tag{18}$$

where α_1 is a numerical parameter of order 1. The first term here is a combination of the first two terms in Eq. (17), because the coefficients $\alpha_{||}$ and $\alpha_{\perp}$ become equal to each other for $Mag_e\to 0$.

For a high magnetization, Mag_e>>1, the expression for the thermal force, up to the terms of the first order in the parameter 1/ Mag_e becomes [18]:

$$\boldsymbol{F}_T = -0.71\nabla_{\|}T_e - \alpha_2\frac{n_e}{Mag_e}\boldsymbol{b}\times\nabla T_e\,, \tag{19}$$

where α_2 is another coefficient of order one. For strong magnetization, the Nernst term is small.

In the case of a weak to order-one magnetization, the Nernst term can be significant and may be dominant over the Biermann battery term, especially if the pressure and the temperature gradient are collinear. The Nernst term in this case is proportional to $\boldsymbol{B}$ (Eq. (18)); by comparing it with the term "1" in Eq. (12), one can say that it describes the magnetic field advection in the direction opposite to the electron temperature gradient (towards lower temperatures). This may be quite important in the plasmas in the confinement mode, like in MagLIF and some of the MTF devices (see [13, 40, 41]), where the plasma is in a quasi-equilibrium state and the hydrodynamic advection is slow (see Sec. 6 below).

We compare the role of the Nernst term (in the un-magnetized case, where it can be quite important, Eq. (18)) and the evolutionary term (the left-hand side of Eq. (12)) by noting that, by

the order of magnitude, the ratio of the two (which we suggest to call "the Nernst parameter", *Ne*) is equal to

$$Ne = \frac{"5"}{|\partial B/\partial t|} \sim \frac{T\tau}{m_e L_\perp^2 \nu_{ei}} \sim \frac{\lambda_{ei} v_{Te} \tau}{L_\perp^2}. \quad (20)$$

The numerical estimate for *Ne* can be written as:

$$Ne \sim \frac{10^{20}[T(eV)]^{5/2}\tau(s)}{Zn_e(cm^{-3})\left[L(cm)\right]^2}. \quad (21)$$

We assume that $T_e \sim T_i = T$.

4. RESISTIVE MHD

If both Nernst, Hall and Biermann terms are small, an equation that describes the magnetic field evolution reads as:

$$\frac{\partial \boldsymbol{B}}{\partial t} = \nabla \times \left[\mathbf{v} \times \boldsymbol{B}\right] + \nabla \times \left[D_M \nabla \times \boldsymbol{B}\right], \quad (22)$$

where **v** is the plasma mass-flow velocity and D_M is magnetic diffusivity (16). This is an equation of the resistive single-fluid magnetohydrodynamics. It has to be solved together with a plasma momentum equation that reads as

$$\frac{\partial \mathbf{v}}{\partial t} + \mathbf{v} \cdot \nabla \mathbf{v} = -\frac{\nabla p}{\rho} - \frac{\left[\boldsymbol{B} \times \nabla \times \boldsymbol{B}\right]}{4\pi\rho} + \nu_s \nabla^2 \mathbf{v} + \nu_b \nabla\left(\nabla \cdot \mathbf{v}\right), \quad (23)$$

where p and ρ are the plasma pressure and density, and ν_s and ν_b are two components of the kinematic viscosity: the "shear" viscosity, ν_s, and the "bulk" viscosity, ν_b. We will focus on the shear viscosity ν_s, having in mind that sheared flows play a dominant role in the problems of magnetic dynamo and field enhancement by the plasma motion.

In a number of dynamical problems related to Z-pinch plasmas the "frozen-in" condition is used that implies that the last term in Eq. (22) is negligibly small. In order for this to be true, the plasma electrical conductivity has to be sufficiently high, so that magnetic diffusivity D_M would be sufficiently low. The magnetic diffusivity (16) can be numerically evaluated as:

$$D_M(cm^2/s) \approx \frac{4 \times 10^6 Z}{[T(eV)]^{3/2}}. \quad (24)$$

The ratio of the first term in the rhs of Eq. (22) to the second term is called the magnetic Reynolds number, $\mathrm{Re}_M = Lv/D_M$, where v is characteristic fluid velocity and L is the length-scale. For large magnetic Reynolds number, the diffusion term is small compared to the advection term, and vice versa. Expressing v in terms of the Mach number and sound speed,

$$v = Mc_s, \quad (25)$$

with $c_S = \sqrt{(Z+1)T/Am_p}$ (in the plasma with $T_e = T_i = T$), one arrives at the following numerical estimate:

$$\mathrm{Re}_M = \frac{LMc_s}{D_M} = 0.25ML(cm)T(eV)^2\sqrt{\frac{Z+1}{AZ^2}}, \quad (26)$$

where L is the length-scale. The partition of the (T, L) plane by the lines of $\left(\mathrm{Re}_M/M\right)\sqrt{AZ^2/Z+1}$ =const is shown in Fig. 6. Again, we introduce the Z- and A-dependent multiplier to make the plot applicable to various species. The magnetic Reynolds number is

particularly significant for the experiments on the laboratory astrophysics of the type described in Ref. 32.

We proceed now to plasma viscosity – a dissipative effect that is present in Eq. (23). At the modest plasma temperatures characteristic of the present astrophysics-related studies, the ions are unmagnetized (see Fig. 1). This allows one to evaluate the plasma shear viscosity ν_s by an equation [18]:

$$\nu_s(cm^2/s) = \frac{2\cdot 10^{18}\left[T(eV)\right]^{5/2}}{A^{1/2}Z^3 n_e(cm^{-3})}. \qquad (27)$$

This quantity is very sensitive to the ion charge and becomes quite small for Z>6. In this case, the admixture of the light species (like hydrogen) may lead to a significant increase of the viscosity. The corresponding effect has been roughly evaluated in Ref. 42 and consistently analysed in Ref. 43.

The hydrodynamical Reynolds number defined as

$$\mathrm{Re} = L\mathrm{v}/\nu_s \equiv LMc_s/\nu_s \qquad (28)$$

is equal to

$$\mathrm{Re} = 5\cdot 10^{-13}\frac{ML(cm)n_e(cm^{-3})Z^3\sqrt{Z+1}}{\left[T(eV)\right]^2} \qquad (29)$$

The Reynolds number is directly related to the ion collisionality (2):

$$\mathrm{Re} \approx MCol\sqrt{Z+1} \qquad (30)$$

Having a correct relation between the two Reynolds numbers, Re_M and Re, is important in the studies of the magnetic dynamo: in most of the astrophysical systems one has $Re_M >> Re$, due to a relatively low density. In the stellar interiors, including the Solar convective zone, however, one can have an inverse condition [44]. The ratio of the magnetic Reynolds number to the viscous Reynolds number is called the Prandtl number,

$$\mathrm{Pr} = \mathrm{Re}_M/\mathrm{Re}. \qquad (31)$$

As is clear from Eqs. (26) and (29), this number is a very strong function of the temperature ($\mathrm{Pr} \propto T^4$) and the ion species ($\mathrm{Pr} \propto 1/Z^4\sqrt{A}$).

Anisotropic ion viscosity is more typical to hot, strongly magnetized plasma, like the one met in the magnetic confinement devices and in some versions of MTF. We briefly discuss the corresponding effects in Sec. 6.7 below.

5. MAGNETIC RECONNECTION IN A DENSE PLASMA

Magnetic reconnection is a process of change of the global topology of the magnetic field within the time much shorter than the resistive diffusion time (a "sudden" change). A cartoon that illustrates one of the most dramatic forms of reconnection first mentioned by E.N. Parker [45] and J.W. Dungey [46]). is shown in Fig. 7. Here two flux tubes in otherwise weakly magnetized plasma are depicted; they are brought together by a slow motion of the ambient plasma (like in a Solar convective zone). When the flux-tubes touch each other at some point and "reconnect" there, a part of the magnetic energy is released by the straightening of each of them. Also, the points that were not connected along the magnetic field lines (say, points 1 and 2 in Fig. 7 become connected.

In the natural environment, reconnection occurs in a variety of astrophysical objects, in particular, in Solar and stellar flares. For the parameters of the transition region between the

Solar photosphere and corona, which plays an important role in the flare events, the plasma temperature is a few electron-volt, and the magnetic diffusion coefficient D_M (24) is $\sim 1.5 \cdot 10^6$ cm^2/s. Taking as a characteristic scale $L \sim 1000$ km, one finds that the resistive time would be $\sim L^2/2D_M \sim 3 \cdot 10^{10}$ s$\sim$ 1000yr (!). In reality, the typical energy release time in the Solar flare is $\sim$ 10 min. In order to explain this huge discrepancy, one needs to find some mechanisms that would cause fragmentation of the initial smooth (with a scale $\sim L$) current distribution into smaller and smaller structures, possibly down to the scales approaching the Debye radius (if the current-driven microturbulence is involved). Local plasma temperature may then increase significantly. There is a remarkable progress in the understanding of the processes underlying the fast energy release (see review [47]), but it is still an area of active research.

Spatial scales that are involved in reconnection include the global scale L, collisional electron-ion mean-free path, λ_{ei}, the ion skin-depth, c/ω_{pi} (equal to the ion gyroradius in the β=1 hydrogen plasma, Eq. (6)), the electron skin-depth, c/ω_{pe}, and, finally, the electron Debye radius $r_{De}=v_{Te}/\omega_{pe}$. For a hydrogen plasma with $n= 10^{12}$ cm^{-3}, T=10 eV, one has λ_{ei}= 300 cm, c/ω_{pi}=30 cm, c/ω_{pe}=0.5 cm, r_{De}=30 μm, so that

$$L >> \lambda > c/\omega_{pi} >> c/\omega_{pe} >> v_{Te}/\omega_{pe}. \quad (32)$$

As one can see, there is a clear separation of scales in this example, allowing the energy to cascade to the smallest scales, where collisionless dissipation would occur.

On the other hand, deeper in the stellar interior, the relation between the spatial scales may be quite different. If one takes, as an example, a middle of the convection zone [44], at the depth of about 0.1 solar radius, where the magnetic fields are, probably, generated, one finds there a plasma with the temperature of $\sim$ 100 eV and density $\sim 10^{22}$ cm^{-3}. The relations between the aforementioned parameters becomes now quite different: the mean-free path becomes only a few times larger than the Debye radius and much smaller than all other scales, except for the global scale. Indeed, one has now $\lambda_{ei}=310^{-6}$ cm, $c/\omega_{pi}=310^{-4}$ cm, $c/\omega_{pe}=510^{-6}$ cm, $r_{De}=10^{-7}$ cm, so that

$$L >> c/\omega_{pi} >> c/\omega_{pe} > \lambda > v_{te}/\omega_{pe}. \quad (33)$$

This means that reconnection under such circumstances, if present, should be completely governed by the resistive MHD phenomena. Most probably, it occurs via formation of smaller-scale hydrodynamical vortices (called in ths context "plasmoids") that would cause enhanced dissipation of the magnetic field [48-50].

These regimes of reconnection may be studied with the Z-pinch plasmas. We would have to use a higher-Z plasma, like carbon, in order to enhance the electron scattering. For L=100 μm (plasma radius after rebound), Z=6, $n_e=10^{21}$ and T=100 eV, we would have λ_{ei}=0.02 μm, c/ω_{pi}=50μm, c/ω_{pe}=0.5 μm i.e., an ordering similar to that met in the stellar convective zones, Eq. (33). Specific design of such experiment goes well beyond the scope of this tutorial.

6. MTF AND MagLIF PLASMAS

6.1 General framework

One of important applications of Z-pinches is a quasi-adiabatic compression of a pre-formed magnetized plasma by an imploding liner. In this scheme, the liner is assumed to be much heavier than the plasma inside, the implosion velocity to be much smaller than the plasma sound speed and the heating to be caused by the *pdV* work performed by the liner on the plasma inside. In the course of implosion the plasma passes through a sequence of mechanical equilibria of a gradually decreasing radius, with the spatial distribution of the plasma parameters determined by the transport processes in this plasma. The plasma beta is typically high, $\beta>1$ and in this respect the situation is quite different than the equilibria in magnetic confinement devices. [Note that the relative slowness of the evolution makes this plasma different also from the inertial confinement plasma.] The fusion concepts employing this intermediate approach are usually termed as MTF (Magnetized Target Fusion) or MagLIF (Magnetic Liner Inertial Fusion). Relative importance of various transport processes in this scheme is quite different from the low-beta plasma. Therefore, we present in this section an overview of transport processes in this high-beta, slowly (in terms of the acoustic time) evolving plasma. To be more specific, we discuss a set of parameters relevant for the MagLIF project, although the same general approach can be used for other configurations involving plasma compression by the liners, in particular, compression of field-reversed configurations [14,15]; for a general review of the field-reversed configurations (FRC) see Ref. [50].

To set the stage for the further analysis of the plasma behaviour, we start from a simple scaling exercise for a purely radial compression. In this scaling we initially ignore the plasma and magnetic flux losses and later evaluate the losses on the thus found background. The logic behind such an approach is that, to be successful, the system has to operate with small losses; therefore, a subsequent check allows us to circumscribe the parameter domain where one can expect a good performance.

We characterize the compression by the radial convergence *C*,

$$C \equiv \frac{r_0}{r} \tag{34}$$

where r_0 and r are the initial and the current radii of the cylindrical cavity. By "initial" we mean the radius at the moment when a pre-plasma was formed. This radius may be slightly less than the radius at the onset of the current pulse [13].

Conservation of particles, entropy, and magnetic flux for the loss-free compression leads to the following scalings:

$$n = n_0 C^2,\ p = p_0 C^{10/3}, B = B_0 C^2,\ T = T_0 C^{4/3}. \tag{35}$$

We see that the magnetic pressure $p_M = B^2/8\pi \sim C^4$ grows faster than the plasma pressure. In order to ensure that the liner *pdV* work goes mostly to the plasma, not to the magnetic field, it is desirable to start implosion from the state where the plasma pressure is several times higher than the magnetic pressure, so that the parameter $\beta \equiv 8\pi p/B^2$ in the initial state is significantly higher than 1. For β, one obviously has:

$$\beta = \beta_0 C^{-2/3}. \tag{36}$$

Assuming, as in Slutz et al. [13], β_0~200, we find that even for a high radial convergence of 30, the final value of β is still high, ~30. Given this consideration, we focus below on a high-beta plasma.

Scaling (35) is related to the hot core plasma, whereas there is always a colder plasma near the walls. We will dwell on some features of this denser plasma further in this sections. Scaling (35) certainly overpredicts the central temperature and density compared to the detailed numetical analyses [13, 40, 41]. Still, it can be quite helpful in a rough identification of transition between various models of plasma transport, magnetic field advection, plasma rotation, etc. in the further sections

Scalings (35) and (36) correspond to a purely radial implosion of a cylindrical plasma with an axial magnetic field. For other magnetic configurations and/or implosion geometries the scaling may be different. In particular, in the FRC imploded by a cylindrical liner, without "push" from the ends, beta averaged over the volume stays at the initial level of β_0~1, and the liner length shrinks slower than the liner radius [52]. Conversely, if the FRC is imploded in a homologous fashion [14], so as to maintain its length-to-radius ratio constant (this requires a "push" from the ends), β increases in the course of compression, $\beta = \beta_0 C$, and one can have a high efficiency of the implosion even starting at β_0~1. However, the homologous implosion requires more complex magnetic configurations and liner shapes than just a cylindrical liner with a uniform axial bias field. Our analysis can be reproduced for these other configurations by changing the *C*-scaling; the general framework remains the same.

For the pressure scaling (35), one has $\dot{p}/p = -(10/3)\dot{r}/r$. The "minus" sign accounts for the fact that compression corresponds to $\dot{r} < 0$. We will characterize the energy losses (thermal conduction and bremsstrahlung) by the loss times τ_{cond} and τ_{rad}. With those taken into account, the pressure evolution equation becomes

$$\frac{\dot{p}}{p} = -\frac{10}{3}\frac{\dot{r}}{r} - \frac{1}{\tau_{cond}} - \frac{1}{\tau_{rad}}, \tag{37}$$

$$\tau_{cond} = \frac{r^2}{6\chi};\ \tau_{rad} = \frac{p}{Q_{rad}}. \tag{38}$$

Here χ is a thermal diffusivity and Q_{rad} is the radiation power per unit volume. The factor "6" in the first equation accounts for the cylindrical geometry (roughly, the square of the first root of the Bessel function of zeroth order). For different stages of the implosion different thermal conductivity models may be valid. We will discuss this in the further sub-sections. For τ_{rad} of a pure DT plasma one has [52]:

$$\tau_{rad}(s) = \frac{2.84\times10^{13}\sqrt{T(eV)}}{n(cm^{-3})}. \tag{39}$$

In order for the plasma heating by the *pdV* work to be efficient, the loss terms in Eq. (37) must be small compared to the heating term, by some significant margin. To characterize the effect of various loss mechanisms, we introduce several dimensionless parameters that have to be large in order to have good plasma confinement. For example, the thermal conductivity to the walls will be characterized by the parameter $Cond = \tau_{cond}\left|10\dot{r}/3r\right|$, see Eq. (37). The parameter *Rad* characterizing radiation losses can be introduced similarly, by replacing τ_{cond} by τ_{rad} (Eq. (39)). The possible redistribution of the plasma along the axis will be characterised by parameter *Ac* (the notation refers to the word "acoustic"), see Sec. 6.5. Other important parameters characterizing the plasma state have been introduced in Sec. 2-4.

As a reference point for the initial plasma state, we take the one similar to that presented in Slutz et al., [13]:

$$\rho_0 = 3mg/cm^3\ (n_0 = 7.2\times10^{20}cm^{-3}),\ T_0 = 300eV,\ B_0 = 30T,$$
$$r_0 = 3mm,\ L=0.5\ cm,\ v_L=5\times10^6\ cm/s \qquad (40)$$

For the liner velocity we take an average value between the plasma formation time and the time a couple of nanoseconds before the rebound. All these parameters are not meant to represent any particular case, just a rough general characterization of typical parameters.

Note that we focus on the hot central part of the plasma that occupies large fraction of the total liner interior. On the other hand, the radial pressure equilibrium of a β>>1 plasma means that near the wall a colder and much denser plasma will be present. In some cases, its properties may become important for the overall consistency of the analysis. We dwell on these issues in Section 6.4.

6.2 Collisionality and magnetization

Following Sec. 2, we characterize the plasma collisionality by the ratio of the length of the pinch, L, to the collision mean-free path λ (the same for the ions and electrons in the DT plasma with $T_e=T_i$). For the scalings (35), one has

$$Col = Col^{(0)}C^{-2/3}, \qquad (41)$$

where subscript "0" refers to the initial plasma. For the reference set of parameters (40), one has $Col^{(0)} \approx 750$. For a 30-fold radial convergence, the parameter Col becomes ~ 100, still large compared to unity. This means that *the parallel transport is collisional at all stages of the implosion*.

The ion magnetization parameter, Mag_i, scales as

$$Mag_i = Mag_i^{(0)}C^2 \qquad (42)$$

For the reference set of parameters, Eq. (40),

$$Mag_i^{(0)} = 0.03, \qquad (43)$$

meaning that the ions are initially un-magnetized (collisional). In the course of implosion, they become magnetized at C=4–5, and, by the time of the maximum compression (C=30), the magnetization becomes significant.

The electrons are magnetized from the outset, with

$$Mag_e^{(0)} = 2. \qquad (44)$$

We emphasize that this discussion relates to the central part of the plasma. Near the walls the plasma remains in the un-magnetized state during the whole implosion.

6.3 Cross-field heat transport

The ions are so highly collisional initially, that, despite the fact they are unmagnetized, their thermal conductivity is smaller than the magnetized electron thermal conductivity. Using equations (2.13), (2.15) from Braginski, one finds that initially

$$\left(\frac{\chi_e}{\chi_i}\right)^{(0)} \approx 20. \qquad (45)$$

The two become equal at $Mag_e = \lambda/\rho_e \sim (m_i/m_e)^{1/4}$. This happens early in the implosion, at C~2. From this point on, the classical cross-field electron thermal conductivity is small. The ion thermal conductivity remains un-magnetized until C~5-6. At the transition point, where Mag_i~1 (C~5), the ion thermal diffusivity is approximately

$$\chi_{i\perp} = 0.38\frac{cT}{eB} \tag{46}$$

where T and B are taken at the transition point (see Eq. 4.40 in Braginski). Note that this, purely classical result is an order of magnitude higher (!) than the canonically-defined Bohm thermal diffusivity,

$$\chi_{Bohm} = \frac{1}{16}\frac{cT}{eB} \tag{47}$$

(see the left part of Fig. 8). The difference is caused by a more-or-less arbitrary introduction of a small coefficient 1/16 in the canonical expression for χ_{Bohm}. Note that drift-wave theory allows for transport coefficients well in excess of (47) (e.g., [29, 54]). Still, Eq. (47) is a commonly accepted reference equation and we will use it as such.

Further on, at C>5, the ion magnetization increases and we enter a regime of magnetized ion thermal conductivity, unless microturbulence develops (see below, Sec. 7).

As mentioned in Sec.6.1, we characterize the role of cross-field transport by the ratio of the first and the second terms in the r.h.s. of Eq. (37). The corresponding dimensionless parameter *Cond* is

$$Cond = \frac{10\mathrm{v}\tau_{cond}}{3r}, \tag{48}$$

where v is the implosion velocity. No power-law representation of *Cond* for the whole implosion process is possible, as the heat conduction regimes change from the electron-dominated process very early in the implosion, to the un-magnetized ion thermal conductivity, and eventually to magnetized ion thermal conductivity. Also, especially in this latter regime, there is a possibility of the onset of drift turbulence which would lead to a Bohm-like heat transport. As the cross-field plasma losses are a main cause of concern for magnetic thermal insulation, we discuss the possible anomalous transport in a separate section, Sec. 7.

Numerical results for the thermal diffusivity for various regimes of the cross-field transport are presented in Appendix A. It is easy to see that their scaling with the convergence C is as follows:

$$\chi_{\perp e,i} = \chi^{(0)}_{\perp e,i} C^{-8/3}; \quad \chi_{Bohm} = \chi^{(0)}_{bohm} C^{-2/3}. \tag{49}$$

The corresponding plots for the reference case (40) are presented in Fig. 8. Using these plots, one can find parameter *Cond* (Eq. (48)) as a function of C. We use a simplified model of the constant implosion velocity; Eq. (38) then yields:

$$Cond = \frac{10}{3}\frac{r_0\tau_{cond}}{r\tau_{imp}} = \frac{5}{9}\frac{r_0 r}{\chi_\perp \tau_{imp}}. \tag{50}$$

The results of using this equation for the thermal conductivity model described by a red line in Fig. 8 are shown in Fig. 9. For reference purpose, shown is also a line corresponding to the Bohm thermal diffusivity (blue line) and to a 10-times Bohm diffusivity (green line). One sees that, for the latter model, the cross-field losses become non-negligible. On the other hand, as will be shown in Sec. 7, the high collisionality of the MagLIF plasma makes so high a value of the cross-field transport improbable.

6. 4 Magnetic field evolution

The radial velocity of the plasma in the MagLIF system is of the order of the liner implosion velocity, v_L, so that the magnetic Reynolds number, defined with respect to the instantaneous radius r, is

$$\mathrm{Re}_M = \frac{r v_L}{D_M}. \tag{51}$$

For the dependences (35), the Re_M scales approximately as C, $\mathrm{Re}_M \approx C\,\mathrm{Re}_M^{(0)}$. For the parameters mentioned in Eq. (40), one has $\mathrm{Re}_M^{(0)} \approx 150$; therefore, the frozen-in condition holds for a core plasma to a high accuracy during the whole implosion. This does not mean, however, that there is no magnetic field redistribution over the cross-section: as there is a continuous heat loss from the peripheral plasma to the walls, the core plasma starts slowly flowing towards the walls, to increase a density there and thereby maintain the pressure equilibrium in the presence of the peripheral cooling (a "cooling flow"). This leads to formation of a dense plasma layer near the walls. The magnetic field is advected by this flow and compressed together with the colder near-wall plasma.

Under the condition of $\partial(nT)/\partial r = 0$, which describes a radial equilibrium in a $\beta>>1$ plasma, there will appear a layer of a very high density near the walls. In this zone, due to large radial temperature gradient, the Nernst effect may become important. As mentioned in Sec. 3.4, it causes advection of the magnetic field towards the area of the lower electron temperature, i.e., towards the walls. At modest conductivity of the walls, the field can soak into the walls, thereby causing some flux loss. The Nernst effect, although significant, does not lead to too strong confinement degradation in the MagLIF plasma (Ref. 13). A similar conclusion was reached in the analysis of another high-beta plasma system with the electron beam heating of the core, see Ref. 55.

6. 5 Parallel heat losses

The parallel acoustic time, $\tau_{\|} = L/2c_s$, determines the time for the plasma to reach a mechanical equilibrium over the axial direction. If the ratio of $\tau_{\|}$ to characteristic radial compression time $r/\dot{r}$ to is large, this means that the plasma does not experience significant parallel redistirbution of mass, and the axial density distribution does not evolve. Conversely, if this ratio is large, the plasma reaches pressure equilibrium in the parallel direction and, if the ends contain holes, may experience a non-negligible parallel outflow. For the corresponding dimensionless parameter that we denote by Ac, one has:

$$Ac = \frac{vL}{2rc_S}. \tag{52}$$

For the most part of the compression phase, where one can use a rough approximation of a constant v, $v = r_0/\tau_{imp}$, one has

$$Ac = \frac{r_0 L}{2rc_s\tau_{imp}} \propto C^{1/3}. \tag{53}$$

In other words, the axial redistribution process is most significant early in the implosion process. For the set of parameters (40), one has $Ac^{(0)} \approx 0.5$. This means that initially we are operating in the transitional regime, where some redistribution of plasma along the pinch takes place.

The parallel electron heat loss is controlled by the length of the system. For the parallel thermal conduction time over the length $L/2$, one can use the following rough estimate: $\tau_{\|cond} = L^2/4\chi_{\|e}$, where $\chi_{\|e}$ is evaluated according to Eq. (A9). The corresponding dimensionless parameter is $Cond_{\|} = (10/3)(\mathrm{v}\tau_{\|cond}/r)$. For a simple model of a constant implosion velocity $\mathrm{v} = r_0/\tau_{imp}$, one has

$$Cond_{\|} = Cond_{\|}^{(0)} C^{-1/3} \tag{54}$$

For the set of parameters (40), and τ_{imp}=70 ns, one has $Cond_{\|}^{(0)} \approx 6$. In other words, the axial heat loss is small during the initial stage of the implosion but may become non-negligible later in the pulse.

The dimensionless parameters characterizing the core plasma confinement are summarized in Table 2. They are defined in a way that their higher values correspond to a better performance of the system.

6.6 Radiative losses

We characterize the effect of radiative losses by the ratio *Rad* of the first to the last terms in the right-hand-side of Eq. (37). In order the radiation losses to be unimportant, this ratio must be large. One has, according to Eqs. (38) and (39):

$$Rad = 9\times 10^{13}\,\frac{\mathrm{v}(cm/s)\sqrt{T(eV)}}{r(cm)n(cm^{-3})}. \tag{55}$$

This equation cannot be used near the turn-around point, where the velocity is small and a different analysis is required (see Ref. [13]). Eliminating also the very early stage of the implosion and using a rough model of v=*const*=r_0/τ_{imp}, one can rewrite Eq. (55) as:

$$Rad = Rad_0 C^{-1/3}. \tag{56}$$

In other words, the role of radiation increases towards the end. However, for the reference case (40) the parameter Rad_0 is large ~40, so that even for C=30 the radiation remains insignificant. [Note that this conclusion relates to a pure DT plasma, without impurities.]

On the other hand, Eq. (55) shows that, if one creates the pre-plasma too early, before the liner has already reached significant velocity, the radiation may lead to a cooling of this initial plasma, before the compression picks up.

Table 2 Main dimensionless parameters used to characterize the plasma confinement

Parameter	Definition	Significance
Cond, Eq. (50)	The ratio of the *PdV* heating rate and cross-field heat loss	Must be large to allow efficient plasma heating.
Rad, Eq. (55)	The ratio of the *PdV* heating rate and radiative heat loss	"
Ac, Eq. (52)	The ratio of the plasma axial redistribution time and the implosion time	If this parameter is large, one does not need to "plug" the ends of the flux-tube
$\mathrm{Re_M}$, Eq. (51)	The ratio of the magnetic diffusion time and the implosion time	Has to be large to avoid magnetic flux loss from the core plasma

Another caveat is that the plasma parameters are strongly non-uniform, varying both in the radial and axial direction, and, as was emphasized in Ref. [55], this may lead to strong radiative losses from the plasma near the boundaries, both radial and axial.

6.7 Plasma rotation

The spontaneous plasma rotation which sometimes adds significantly to uncertainties in the predictions of the plasma behavior is easily predictable for the MagLIF: as the plasma is in a direct contact with the end walls (along the axial field lines), the electrostatic potential of the plasma core is on the order of the floating potential, $\sim 2T_e/e$. This sets the $E \times B$ rotation at a low level $v_{rot} \sim v_{Ti}(\rho_i / r)$. This slow rotation cannot have a significant effect on the plasma confinement (unless the plasma beta becomes higher than $(r/\rho_i)^2$). Note that, due to the strong ion magnetization at the later stages of the implosion, the collisional viscous effects become insignificant. Note also that in the systems with closed field lines, like the FRC, the rotation velocity can in principle be much higher, approaching the sound speed and thereby affecting gross plasma stability.

6.8 Impuruty shielding

For the plasma that is in direct contact with the liner an important issue is that of the transport of heavier impurities from the wall towards the plasma core. The inner surface of the liner is ionized by a very high heat flux from the compressed plasma inside and the ions of the wall material can be pulled into the plasma by the effect of the thermal force in the un-magnetized region near the walls. This effect has been considered in Ref. 55. The impurity ions experience the thermal force exerted not only by the electrons but also by the plasma ions. The latter contribution is actually dominant near the walls, where the plasma ions are not magnetized, whereas the electrons are [56].

In the un-magnetized zone of a relatively cold plasma near the wall the thermal force acting on the impurity ions scales as Z^2 [56] and is directed inward, towards the hotter plasma. This creates an impurity ion flow whose velocity is determined by the balance of the thermal force and the friction force against the plasma ions. This might have created a serious problem for the plasma life-time but, fortunately, the ions become magnetized as soon as they get to a slightly hotter plasma closer to the core.

To provide somewhat more detailed description of the processes involved, we introduce the charge and the atomic mass of the impurity, Z_{imp} and A_{imp}, as well as an atomic mass for the fuel made of hydrogen isotopes, A_H, which is equal to 2 for deuterium and 2.5 for the equicomponent mixture of deuterium and tritium. The impurity ions have to have a low concentration as otherwise the radiative losses become too high. We therefore consider them as test particles and account only for their collisions with the fuel particles. As the impurity ions are heavy, each 90-degree scattering event for the plasma ion leads only to a small-angle scattering of the impurity ion. Therefore, the 90-degree scattering of the impurity ion requires time

$$\tau_{imp} \approx \frac{\lambda_H}{v_{TH}} \frac{A_{imp}}{A_H Z^2}. \qquad (57)$$

The ion cyclotron frequency for the impurity ions is $\omega_{Cimp} = \left(Z_{imp} A_H / A_{imp}\right) \omega_{CH}$ so that the magnetization parameter for the impurity ions is

$$Mag_{impurities} \approx Mag_H / Z_{impurities} . \quad (58)$$

We see that, with the increasing distance from the wall, the hydrogen is magnetized first, followed by magnetization of impurities.

The thermal force acting on the impurity ions is determined by the distribution function of the fuel ions and drops rapidly when the latter get magnetized. Moreover, further from the wall the effect of the cooling flow (Sec. 6.4) becomes significant, and the impurities get entrained by this flow that prevents them from entering the hot plasma core. The interplay of these two effects leads to the impurity accumulation in a narrow layer near the wall, without any direct impurity effect on the core plasma. The quantitative description of this phenomenon is presented in Ref. 56.

7. ANOMALOUS HEAT TRANSPORT

As mentioned above, the meso-scale plasma turbulence driven by the gradients of temperature, density and the magnetic field can lead to the diffusion coefficients significantly exceeding the Bohm diffusion coefficient (47). By the "mesoscale" we mean perturbations whose scale length is greater than the ion gyro-radius but smaller than the gradient scale length $L_\perp$ for the temperature, density and the magnetic field (e.g., $L_{\perp T} = T/|\nabla T|$ for the temperature gradient scale length). In particular, analysis of Ref. [29] has shown that in a high-beta *collisionless* plasma the drift instabilities can give rise to diffusion coefficient that is ~ 10 times higher than D_{Bohm}. This would lead to significant heat losses from the MTF/MagLIF plasmas, even for the implosion times as short as in MagLIF.

The characteristic frequency of these mesoscale modes is drift frequency, $\omega_D = cTk_\perp / eBL_\perp$, where $k_\perp$ is the component of the wave number perpendicular to both the magnetic field and the gradient (in the cylindrical geometry this would be an azimuthal component of the wave number). Usually the main contribution to the anomalous transport comes from the largest-scale modes, with $k_\perp \sim 1/L_\perp$ [54], for which

$$\omega_D = \frac{cT}{eBL_\perp^2} . \quad (59)$$

The most unstable perturbations are strongly elongated along the field lines, with $k_{||} \sim 1/L_{||} << 1/L_\perp$ [54].

Table 3 Parameters related to collisional effects in the drift-wave turbulence

The system*	*T (eV)*	*n (cm^{-3})*	*B (T)*	$L_\perp$ *(cm)*	$L_{||}$*(cm)*	ε Eq. (60)	1/*Col* Eq. (2)
1	10^3	$4\cdot10^{22}$	$2\cdot10^3$	$4\cdot10^{-2}$	0.5	$6\cdot10^{-6}$	10^{-4}
2	10^4	10^{14}	5	200	20000	12	10^2

* "1" is a MagLif system half-way into implosion, for the convergence C~8; "2" is a generic mid-size tokamak. Note the difference in the collisionality parameters ε and 1/*Col*.

Due to high plasma densities typical of the Z-pinch plasmas, the drift frequency (59) can be significantly smaller than the ion collision frequency $1/\tau_{ii}$, and the mean free path can be much smaller than $L_{||}$. The condition $\omega_D \tau_{ii} = \varepsilon << 1$ for an equicomponent DT plasma can be represented numerically as:

$$\varepsilon \equiv \frac{2.4 \cdot 10^{10} \left[T(eV)\right]^{5/2}}{n(cm^{-3}) B(T) \left[L_{\perp}(cm)\right]^2}, \tag{60}$$

whereas the condition of the strong collisionality for the parallel dynamics, $k_{||}\lambda_{ii}<<1$. for $k_{||}\sim 1/L_{||}$ is equivalent to the condition $Col = L_{\|} / \lambda_{ii} >> 1$ that is described by Eqs. (1), (2). Taking as an example the MagLIF plasma half-way through the implosion, at $C\sim 8$, one has $T\sim 1$ keV, $n\sim 4\times 10^{22}$ cm^{-3}, $L_{\perp} \sim 0.04$ cm, and $\varepsilon \sim 10^{-5}$. Note that for a typical magnetic confinement devices the parameters ε and $1/Col$ are not small but rather very large. A comparison of some generic tokamak with characteristic parameters of MAGLIF systems is presented in Table 2.

The smallness of parameters ε and $1/Col$ means that the mesoscale turbulence has to be described by *collisional* drift instabilities that are quite different from the *collisionless* instabilities considered in Ref. [29], especially in a high-beta plasma. This analysis has been performed in Ref. [30] and has led to a conclusion that in the regime of ε, $1/Col << 1$, the diffusion coefficient is smaller than the Bohm diffusion coefficient (47) by a factor of 3-5. According to discussion of Sec. 6.3, this would make anomalous cross-field transport in the MagLIF-MTF setting relatively unimportant.

Another and quite different type of instability can be driven by the axial heat flux to the cold end-walls. This instability was considered in Ref. 57 (see also Ref. 58) for the initially un-magnetized plasma; it leads to a spontaneous growth of magnetic perturbations. If in the unperturbed state there are collinear temperature and density gradients (along z), then the Biermann battery effect is absent and the magnetic field is not generated. However, as pointed out in Ref. 57, this state may be unstable with respect to perturbations with the wave vector perpendicular to the common direction (say, z) of the density and temperature gradient. The feedback loop works then as follows: imagine that there appeared a perturbation of the magnetic field $\delta B_y(x)$ directed along y and varying along x. This field would then create a heat flux and the corresponding temperature gradient in the x direction by virtue of the Leduc-Righi effect (an effect thermodynamically conjugate to the Nernst effect) that drives the heat flux in the direction perpendicular to both the temperature gradient and the magnetic field (see, e.g. text [35]). This effect in a fully ionized plasma is described by Eq. (4.33) of Ref. 18:

$$\delta q_{ex} = \chi_{\wedge} \delta B_y \frac{\partial T_e}{\partial z} \tag{61}$$

where δB_y is the magnetic field perturbation and δq is an associated perturbation of the electron heat flux. An expression for $\chi_{\wedge}$ has to be taken for the limit of a weak magnetization (as initially there is no magnetic field):

$$\chi_{\wedge} \approx 5.5 \frac{e n_e T \tau_{ei}^2}{m_e^2 c} \tag{62}$$

(see Eq. 4.37 and Table 2 in Ref. 18).

Since the magnetic field perturbation varies along x, so does the heat flux, thereby creating a temperature gradient in the x direction. This temperature gradient then couples with the unperturbed axial density gradient (along z) by the Biermann battery mechanism,

$\nabla n_e \times \nabla \delta T_e$, and may enhance the seed (y) component of the magnetic field. It turns out that this happens if the unperturbed density and temperature grow in the same direction; if the temperature grows in the direction opposite to the density, perturbations damp. A formal description of this interesting effect can be found in Ref. 57. There are no analyses of the similar instability in the presence of an axial magnetic field available at present.

8. SIMILARITY AND SCALING LAWS

Scaling relations allow one to extrapolate the experimental results from one experiment to another, e.g. from a smaller and less expensive experiment to a larger and more expensive one at the planning stage for the latter. One can also apply this approach to the studies of the laboratory astrophysics, where the scaling will be made between a natural astrophysical phenomenon and a laboratory experiment.

A textbook example of similarity is the Reynolds similarity (see e.g. Ref. [59]) for the flow of incompressible viscous fluid past a rigid body immersed into this fluid. The flow can be characterized by its velocity u at the infinity, fluid mass density ρ and fluid kinematic viscosity ν. The body is characterized by its scale size L. Hydrodynamic equations describing this flow when written in a non-dimensional form, with the dimensions normalized to L and velocities normalized to u turn out to be identical between the two systems, which may be different in the size of the body and flow velocity, provided the Reynolds number $\mathrm{Re}=uL/\nu$ is the same between the two systems. An important additional requirement for this similarity is the geometrical similarity of the system: the shape of the bodies has to be the same (up to the scale transformation), and the orientation of the body with respect to the incoming flow must be the same as well.

The flow that is uniform and steady at the infinity may become non-steady and turbulent around the body and in the wake. If the time-scales are normalized to L/u, then all the statistical spatio-temporal characteristics of the turbulence become identical between the two systems. The stresses at the surface (both normal and tangential components) will be distributed identically over the surface: their magnitude will scale as $\rho u^2 f(\mathrm{Re})$, where f is some function of the Reynolds number. This function cannot be found from the similarity arguments alone: it has to be determined from the solution of the hydrodynamic equations (or from experiment). However, if the Reynolds numbers between the two systems are the same, this latter part becomes unnecessary: the distribution of stresses measured in one system (say, the smaller one) could be immediately predicted for the other (larger) system.

In more complex systems the number of dimensionless parameters that need to be held constant in order to make two systems similar (i.e., described by the identical non-dimensional equations) can be larger than one. What is important for the similarity exercise to be useful is that this number be less than the number of constituent parameters (like u, L and ν in the aforementioned example). If the number of constraints is equal to the number of constituent parameters, the system becomes "stiff": only the systems with the same parameters will behave similarly (in this case identically).

If one tries to find similarities for all-encompassing plasma models, that would include plasma kinetics, radiation and atomic processes, one usually encounters this "stiff" situation. In order to avoid it, one should identify the most important processes and parameters governing the phenomenon of interest and find out whether reduced models can be used. For example, if one is interested in some large-scale hydromagnetic phenomenon in astrophysics, one can assume that

this phenomenon can be described by the set of single-fluid MHD equations (Sec. 4). Then, one has to make sure that the laboratory counterpart is also correctly described by the single-fluid MHD equations and, in particular, that the Hall terms are subdominant (Sec. 3). The further step would be the comparison of the magnetic and viscous Reynolds numbers for both systems. If one is interested in the ideal MHD effects, not involving in a significant way the turbulent magnetic field generation/amplification, one can just require that both Reynolds numbers are much greater than unity (say, 50). Then one enters the domain of an ideal magnetohydrodynamics, which has a very broad class of similarities ("Euler similarities" described in Refs. 11, 60, 61) that allow for the presence of shocks and turbulence (the latter in a non-dissipative range of scales). To use this similarity in its strict form one would have to take care of the geometric similarity and the similarity of the hydrodynamic characteristics (e.g., the ratio of the ram pressure and gas pressure, as well as magnetic pressures at the characteristic point(s). Dependence on the (large) Re and Re_M drops out and their specific values become unimportant, unless one wants to consider turbulence down to dissipative scales.

A number of astrophysics-related laboratory experiments have successfully used the Euler magnetohydrodynamic scaling that is based on the assumption that both hydrodynamic and magnetic Reynolds numbers are large. To give the reader some idea of the scope of these experiments, we mention a few of them. In Ref. 32, magnetically-driven tower jets were generated by the conical wire arrays and their deflection by the plasma "cross-winds" was discovered. In the same paper, magnetically-supported "tower jets" were produced from the radial wire arrays. In Ref. 62 the jets were produced from a thin disk electrode. Plasma rotation was studied in Refs. 32 and 63. Astrophysics-relevant bow shocks were produced in nested wire arrays [64], where radiatively-cooled plasma streams ablated from the outer wires would flow around the wires of the inner array. It turned out that highly collimated, high-Mach-number jets can be produced also by a relatively low-current X-pinch discharges [65, 66]. Sheared flows were produced and studied in Ref. 67. In all these studies the scaling to real astrophysical objects was discussed.

Now we switch to the possible use of scaling analysis to the fusion plasma confinement in MagLIF-MTF systems. In magnetic confinement research there is a long history of using similarity criteria for the studies of the plasma behaviour, Refs. 68-70. Recently a similarity analysis was done also in conjunction with the MagLIF plasma [10]. Here we discuss a simplified version of this scaling, assuming that the DT plasma is confined in an infinitely long cylinder. Then, one would be concerned with the radial plasma confinement against the cold walls. The plasma is immersed in an axial magnetic field and held together by a highly conducting walls at the radius a. We consider an initial value problem. In other words, we assume that the cylinder is filled with a plasma of a certain temperature and density, permeated with a pre-imposed axial magnetic field. If this initial plasma is "set free" at t=0, it starts evolving, losing heat and redistributing density, temperature and the magnetic field to maintain the radial equilibrium.

We consider here the case where the plasma is sufficiently collisional, so that the plasma lifetime is much longer than the electron-ion temperature equilibration time (3). In this case, one can characterize the fully ionized, single ion species plasma (we take m_i=2.5m_p) by such parameters as temperature and particle density. These quantities, as well as the magnetic field. evolve according to collisional two-fluid equations [18]. These equations allow for the development of small-scale instabilities, in particular, drift-type instabilities of Sec. 7 and other instabilities that are described by the two-fluid equations. Applicability condition is that the

characteristic fluctuation time is significantly longer than the ion collision time. With that, anomalous transport discussed in Sec. 7 is covered by this similarity. The initial state is that of the mechanical equilibrium, so that the radial particle velocity is zero.

To find the invariance (similarity) properties, one can introduce dimensionless variables, measuring the density, temperature and the magnetic field in the units of their initial values on axis, normalizing the spatial scales to a, and temporal scales to the ion crossing time, $t_c=a/v_{Ti}$. The dimensionless quantities then become:

$$\hat{n}=\frac{n}{n_0};\ \hat{T}=\frac{T}{T_0};\ \hat{\boldsymbol{B}}=\frac{\boldsymbol{B}}{B_0};\ \hat{\boldsymbol{r}}=\frac{\boldsymbol{r}}{a};\ \hat{t}=\frac{t}{t_c}\ . \tag{63}$$

The electron and ion velocities that appear in the course of the temporal plasma evolution are normalized to a/t_c. Note that the scale t_c is just the normalization parameter, not the confinement time (which is much longer).

As shown in Ref. [10], if written in terms of these non-dimensional quantities, the Braginski equations are invariant between two plasmas, provided the following three dimensionless parameters are the same between the two systems: the ion magnetization (6), the plasma collisionality (2) with $L=a$, and the plasma beta (7), all evaluated for the initial parameters on axis. In other words, for a similar initial radial distributions, there are *four* dimensional input parameters, n_0, T_0, B_0 and a that may vary between the two systems and there are *three* constraints on them: *Mag*=const, *Col*=const, β=const. In other words, the system is not "stiff," and one can consider similarly behaving systems of different radii. If one changes the radius and maintains the scaling parameters constant, the plasma parameters and the magnetic field in the initial state have to be adjusted accordingly (like in the Reynolds similarity: changing the scale L when keeping the Reynolds number constant, means that the fluid velocity u has to be changed as $1/L$). Note that in the plasma with $T_e=T_i$ the constancy of *Mag* and *Col* for the ions means the constancy of the same parameters for the electrons (see Eqs. (2, 6)); to be specific, we speak here about the ions.

To see what variations of the plasma parameters are allowed if the three scaling parameters are kept constant and the plasma radius a changes from one experiment to another, one has to solve three equations, *Mag*=const, *Col*=const, and β=const, for three quantities, n_0, T_0, B_0, with a varying. In this way we find that

$$T_0 \propto a^{-1/2}\ ,\ n_0 \propto a^{-2}\ ,\ B_0 \propto a^{-5/4}\ . \tag{64}$$

Surprisingly, it may be easier to imitate the millimetre-scale MagLIF targets by larger scale, lower density and magnetic field plasmas that would be easier to diagnose.

The initial-value problem formulated above is not quite the same as that of the evolution of a continuously *PdV*-heated target in the MTF approach. Introducing the continuous heating destroys the similarity – the system becomes "stiff." On the other hand, as suggested in Ref. 9, the decay of an initially-created plasma allows one to get an idea of the plasma life-time at given initial parameters. To be compatible with the *pdV* heating, this life-time has to be longer than the heating time at a given stage of the implosion. Therefore, the decay experiments and their scaled versions would allow one to assess, in a piece-meal fashion, the feasibility of the whole implosion process.

As is typically the case in the plasma-scaling exercises, the inclusion of the radiation losses destroys the plasma similarity. Indeed, one can check (see Ref. 10) that scaling of the radiation terms would introduce one more similarity constraint (the fourth) thereby making the system "stiff" (the scaled system must be identical to the original one).

9. ENERGETIC PARTICLES AND BEAMS

This subject falls out of the general area of collisional plasma physics covered by this review, so we will provide only very short summary with a few references.

The formation of particle beams seems to be a natural process in the Z-pinch geometry due to a possibility of the current break-up in the course of development of a sausage instability. The rapid development of the "neck" causes formation of high electric fields in the direction of the pinch current. On the axis, the magnetic field is zero, and the electrons can be freely accelerated towards the anode, provided the electric field exceeds the runaway limit [71], at least for the higher-energy tail. If the disruption occurs in a non-symmetric way, of importance is the length of the field line segments over which an integral $\int E_{\|} dl$ has significant value. After having been accelerated in this zone, the electrons can travel further along the magnetic field lines and away from the disruption area. Their general direction would be towards the anode. Similar mechanism can work for the ions: the ions accelerated to high energies in the constriction can become weakly collisional and propagate to the cathode. Due to the much larger ion mass, the ions do not necessarily follow the magnetic field lines and their trajectories in the constriction area may be quite complex (M. Haines, Ref. 72).

Deutsch and Kies (Ref. 73) considered ion acceleration resulting from the multiple ion reflections from the cylindrical "mirror" collapsing on axis. The "mirror" is a model of a steeply increasing magnetic field. If the plasma in front of a "mirror" is not too dense, the ions do not scatter between the two successive reflections, and a kind of an ion runaway occurs. In this case, there is no strong anode-cathode asymmetry of the ion distribution. Trubnikov considered the ion acceleration by their "squishing" out of the rapidly narrowing "neck" (Ref. 74). Recent analyses of the formation of the ion tails in the pinch constriction, as well as a summary of experimental results is presented in a comprehensive review by Vikhrev and Korolev (Ref. 75). A progress in increasing the number of fast deuterons for the neutron production in Z pinches has been reported by D. Klir et al. [**76**]. Interestingly, the generation of fast particles was observed also in laboratory astrophysics experiments [**77**], where the protons with the energies significantly exceeding the applied voltage were detected in the geometry of magnetic tower jets.

Yet another mechanism of the fast ion generation may be related to the particle acceleration by microturbulence. The latter would naturally develop when the velocity of the current-carrying electrons in the constriction exceeds the threshold for the current-driven electrostatic instability. This would be an ion-acoustic or Buneman-like instability, depending on the electron-to-ion temperature ratio. The microturbulence develops at the scale of a few Debye radii and has frequencies of order of the ion plasma frequency. In the plasmas of Z-pinches, with the constriction densities in the range of 10^{19}-10^{20} cm^{-3} electrostatic turbulence can lead to rapid acceleration of the "tail" ions initially having energy of a few ion temperatures. The maximum attainable energy would be limited by the size of the ion gyro-orbits in the magnetic fields near the current "neck." Ion acceleration by the microturbulence favours the direction in which the ion acoustic waves are propagating (in the direction of the electron flow), i.e., towards anode.

A combination of these effects may give rise to a very dynamic picture of the energetic particles in the form of the mixture of the particle beams and quasi-isotropic "tail" particles. A lot of experimental information regarding the fast particle generation has been obtained in the studies of plasma foci, where the acceleration may occur in multiple points, after the current break-up to many filaments, merging and disrupting in an intricate "dance" [9].

In recent years, advanced computing capabilities have allowed to self-consistently assess aforementioned mechanisms [78], except, possibly, the one related to the current-driven electrostatic microturbulence [2].

A topic somewhat related to the behaviour of fast particles is that of the dynamics of fusion alpha-particles that would be generated in the MagLIF-MTF plasmas [40, 41]. If the imploding liner impresses asymmetries on the field inside it, their dynamics may become quite complex. The dominance of the axial field makes the dynamics of alpha particles in this system more predictable than the fast particle behaviour in the systems with current disruptions.

10. CONCLUSIONS

This tutorial focuses on those issues of the plasma physics that are particularly important in the Z-pinch environment. Although the basic plasma properties for most of the regimes typical of the Z pinches are well known, the application of the existing plasma models to highly-dynamical plasmas of Z pinches requires a thoughtful use of these models. This paper may help researcher to identify the parameter domain in which particular effects or particular models would play a dominant role. The use of dimensionless parameters characterizing the relative strength of various effects can be of a significant help in this regard. Table 4 summarizes a few most important parameters used throughout this article.

The resistive MHD covers a lot of situations involving a relatively cold plasmas of the imploding liners. This reduced way of description may also be helpful in simulating large-scale astrophysical phenomena occurring in collisional plasmas. MHD turbulence in a collisional plasma can also be described by the single-fluid MHD. There are situations (mostly in dense, nearly non-ideal plasmas) where MHD reconnections are governed by the nonlinear tearing instabilities described by the resistive single-fluid MHD. Constraints for the single-fluid MHD come usually from the need to account for the Hall effect that becomes important at higher currents and lower plasma densities (high relative velocities of the electrons and ions).

The two-fluid description is needed to account for the Nernst effect and to assess transport properties in relatively slowly evolving plasmas, like the magnetized target fusion plasma held in a quasi-equilibrium state by the liner walls. In this confinement problem one encounters a situation where the plasma magnetization changes from very high values near the axis to very low values in a cold dense plasmas near the walls, thereby involving quite different transport models. The highly magnetized zone may be subject to drift-type instabilities and enhanced transport, but the instability shows up in a collisional version and leads to transport coefficients below the reference Bohm value. Interestingly, there exists a broad similarity covering the two-fluid description for the case where the electron and ion temperatures are equal (i.e., for the processes occurring at the time-scale longer than the electron-ion equilibration time).

In the situation where the current path is disrupted by the development of the larger-scale instabilities, one can encounter the situations where suprathermal particles are formed, either in the form of the beams or quasi-isotropic “tails” of the particle distribution. These effects are particularly prominent in the plasma focus settings. Likewise, the magnetic reconnections in an ideal plasma may manifest transition to smaller and smaller scales, down to collisionless anomalous phenomena. This interesting and important phenomenon is, however, only barely touched upon in this tutorial focused mostly on collisional systems.

Generally, the physics of Z-pinch plasmas is a rich and rapidly advancing area of plasma physics; given its fundamental value and numerous applications, it certainly deserves more attention of a broader plasma physics community.

Acknowledgments

The author is grateful to Professor F. Beg for the continuing and patient encouragement and to Professor S.V. Lebedev for illuminating discussions. This work was performed under the Auspices of the U.S. Department of Energy by Lawrence Livermore National Security, LLC, Lawrence Livermore National Laboratory, under Contract DE-AC52-07NA27344 with support from Sandia National Laboratories.

Table 4 Main dimensionless parameters

Notation, Eq. number	Name and verbal definition	Significance
Col Eq. (2)	*Collisionality* The ratio of the spatial scale and the particle m.f.p.	Most important for the parallel (with respect to magnetic field) plasma dynamics; for large collisionality the electron heat transport is diffusive; the Maxwellian ion "tails" are not depleted by fast parallel losses. Due to the Z^4 dependence of the *i-i* collision cross-section, the collisionality can be much higher for the ions than for the electrons. The parameter Col is also related to the ratio of the plasma evolution time and the particle collision time.
$Mag_{e,i}$ Eq. (5)	*Magnetization* The ratio of the gyrofrequency to the collision frequency (equal to the ratio of the m.f.p. to the gyroradius)	If large, means that in every scattering event the particle shifts across a magnetic field by roughly a gyro-radius. At equal electron and ion temperatures is higher for the elctrons than for ions. Affects cross-field transport and magneto-thermal effects.
β Eq. (7)	*Plasma "beta"* The ratio of the plasma pressure to the magnetic pressure	Large *beta* signifies that the magnetic field does not have significant effect on the gross dynamics of the plasma, although may still be important for the plasma transport if the magnetization $Mag_{e,i}$ is high. Is approximately equal to the square of the ratio of the sound speed and the Alfven velocity.
Ha Eq. (14)	*Hall parameter* The ratio of the "current" velocity (*e* vs. *i*) to the flow velocity	If large, means that the magnetic field is advected with velocity different from that of the hydrodynamic flow; at large *Ha*, the system is prone to development of the smaller-scale instabilities.
Ne Eq. (20)	*Nernst Parameter* The ratio of the magnetic field evolutionary time to the thermal advection	For large *Ne*, the presence of the thermal advection of the magnetic field may dominate resistive diffusion and nydrodynamic advection. In the plasma with $Mag_e<1$ the advection is directed towards the areas of lower electron temperature
M Eq. (25)	*Mach number* The ratio of the flow velocity to the sound speed	High Mach numbers usually mean that strong shocks, collisional or collisionless, can be present in the system.
Re Eq. (28)	*Reynolds number* The ratio of the viscous time and the convective time	Large *Re* means that ideal hydrodynamics is applicable for a large range of scales, from the global scales to the dissipative scales (but not the dissipative scales themselves).
Re_M Eq. (26)	*Magnetic Reynolds number* The ratio of the resistive diffusion time and the convective time	Large Re_M means that the magnetic field is frozen into the plasma to a high accuracy; the line-tying breaks down only at small scales (the smaller, the higher Re_M). Sometimes, a so called Lundquist number is used (instead or in parallel with Re_M), where the convective velocity is replaced by the Alfven velocity.
Pr Eq. (31)	*Magnetic Prandtl number* The ratio Re_M/Re	This number is important in the studies of a turbulent magnetic dynamo.

Appendix. Useful numerical relations for the DT plasma (Z=1, A=2.5)

Electron density in an equi-component DT plasma:

$$n(cm^{-3}) = 2.4 \cdot 10^{20} \rho(mg/cm^3) \tag{A1}$$

Plasma beta:

$$\beta = 8 \cdot 10^{-20} \frac{n(cm^{-3}) T(keV)}{B^2(MG)} \approx 20 \frac{\rho(mg/cm^3) T(keV)}{B^2(MG)} \tag{A2}$$

Conversely,

$$B(MG) = 4.4 \sqrt{\frac{\rho(mg/cm^3) T(keV)}{\beta}} \tag{A3}$$

The ion gyro-radius:

$$\rho_i(cm) \approx 7.6 \cdot 10^{-3} \frac{\sqrt{T(keV)}}{B(MG)} \approx 1.7 \cdot 10^{-3} \sqrt{\frac{\beta}{\rho(mg/cm^3)}} \tag{A4}$$

The electron gyro-radius:

$$\rho_e(cm) \approx 1.1 \cdot 10^{-4} \frac{\sqrt{T(keV)}}{B(MG)} \approx 2.8 \cdot 10^{-5} \sqrt{\frac{\beta}{\rho(mg/cm^3)}} \tag{A5}$$

The ion mean-free path (equal to the electron mean-free path in a Z=1 plasma)

$$\lambda_i(cm) = 3.3 \cdot 10^{18} \frac{T^2(keV)}{n(cm^{-3})} = 1.4 \cdot 10^{-2} \frac{T^2(keV)}{\rho(mg/cm^3)} \tag{A6}$$

The ion magnetization parameter:

$$\frac{\lambda_i}{\rho_i} = 4.3 \cdot 10^{20} \frac{T^{3/2}(keV) B(MG)}{n(cm^{-3})} = 8.2 \frac{T^2(keV) \sqrt{\beta}}{\sqrt{\rho(mg/cm^3)}} \tag{A7}$$

The magnetic diffusivity (in this equation we retain the Z-dependence):

$$D_M(cm^2/s) \approx \frac{4 \times 10^6 Z}{[T(eV)]^{3/2}} \tag{A8}$$

We consider a plasma with $T_e=T_i=T$, $n_e=n_i=n$, so that the energy per unit volume is $3n_eT$; accordingly, the electron and ion thermal diffusivities that enter equation $\partial T/\partial t = \left(\chi_e + \chi_i\right)\nabla^2 T$ are related to the thermal conductivities κ_e and κ_i presented in Ref. [18] as $\chi_{e,i} = \kappa_{e,i}/3n$.

Parallel electron and ion thermal diffusivities:

$$\chi_{\|e}(cm^2/s) = 6.5\times10^{19}\frac{T^{5/2}(eV)}{n(cm^{-3})};\ \chi_{\|i}(cm^2/s) = 1.7\times10^{18}\frac{T^{5/2}(eV)}{n(cm^{-3})} \qquad \text{(A9)}$$

Perpendicular electron and ion thermal diffusivities:

$$\chi_{\perp i}(cm^2/s) = 5.1\times10^{-15}\frac{n(cm^{-3})}{B^2(MG)\sqrt{T(eV)}} \qquad \text{(A10)}$$

$$\chi_{\perp e}(cm^2/s) = 2.52\times10^{-16}\frac{n(cm^{-3})}{B^2(MG)\sqrt{T(eV)}} \qquad \text{(A11)}$$

Bohm diffusivity $\chi_{Bohm} \equiv (1/16)(cT/eB)$:

$$\chi_{Bohm}(cm^2/s) \approx 6.2\frac{T(eV)}{B(MG)} \qquad \text{(A12)}$$

Alpha-particle slowing-down time on the elwcreons:

$$\tau_\alpha(ns) \approx 10^{21}\frac{\left[T(keV)\right]^{3/2}}{n(cm^{-3})} \qquad \text{(A13)}$$

References

1. A.C. Kolb. “Magnetic Compression of Plasmas.” Rev. Mod. Phys., **32**, 748 (1960).
2. D.D. Ryutov, M.S. Derzon, M.K. Matzen. “The physics of fast Z pinches.” Rev. Mod. Phys., **72**, 167 (2000).
3. M. G. Haines. “A review of dense Z-pinches.” Plasma Phys. Controlled Fusion, **53**, 093001 (2011).
4. M.K. Matzen, “Z pinches as intense x-ray sources for high-energy density physics applications.” Phys. Plasmas, **4**, 1519 (1997).
5. M.E. Cuneo, Waisman, EM; Lebedev, SV Chittenden, JP; Stygar, WA Vesey, et al. “Characteristics and scaling of tungsten-wire-array z-pinch implosion dynamics at 20 MA” Phys. Rev. E, **71**, 046406 (2005).
6. Kantsyrev, V. L.; Chuvatin, A. S.; Safronova, A. S.; et al. “Radiation sources with planar wire arrays and planar foils for inertial confinement fusion and high energy density physics research.” Phys. Plasmas, **21**, 031204 (2014).
7. T.A. Shelkovenko, S.A. Pikuz, C.L. Hoyt, et al. “Study of New Configurations of Hybrid X Pinches” IEEE Trans. on Plasma Sci, **42,** 748 (2014).
8. F.N. Beg, R.B. Stephens, H-W Xu, D. Haas, S. Eddinger, G. Tynan, E. Shipton, B. DeBono, K. Wagshal. “Compact X-pinch based point X-ray source for phase contrast imaging of inertial confinement fusion capsules.” Appl. Phys. Lett., **89**, 101502 (2006).
9. P. Kubes, D. Klir, J Kravarik, K Rezac, J Kortanek, V Krauz, K Mitrofanov, M Paduch, M Scholz, T Pisarczyk, T Chodukowski, Z Kalinowska, L Karpinski and E Zielinska.” Scenario of pinch evolution in a plasma focus discharge.” Plasma Phys. Control. Fusion, **55**, 035011 (2013).
10. D.D. Ryutov, M.E. Cuneo, M.C. Herrmann , D.B. Sinars , S.A. Slutz. “Simulating the MagLIF plasma confinement with smaller-scale experiments.” Phys. Plasmas, **19**, 062706, (2012).
11. D.D. Ryutov, R.P. Drake and B.A. Remington. “Criteria for scaled laboratory simulations of astrophysical MHD phenomena.” Astrophysical Journal - Supplement, **127**, 465 (2000).
12. B.A. Remington, R.P. Drake, D.D. Ryutov, "Experimental astrophysics with high-power lasers and Z pinches", *Rev. Mod. Phys.,* **78,** 755 (2006).
13. S. A. Slutz M. C. Herrmann, R. A. Vesey, A. B. Sefkow, D. B. Sinars, D. C. Rovang K. J. Peterson, and M. E. Cuneo. “Pulsed-power-driven cylindrical liner implosions of laser preheated fuel magnetized with an axial field.” Phys. Plasmas, **17**, 056303 (2010).
14. R.P. Drake, J.H. Hammer, C.W. Hartman, L.J. Perkins, D.D. Ryutov. “Submegajoule Liner Implosion of a Closed Field Line Configuration,” *Fusion Technology*, **30**, 310, (1996).
15. J.H. Degnan, M. Amdahl, M. Domonkos, F.M. Lehr, C. Grabowski, P.R. Robinson, E.L. Ruden, W.M. White, G.A. Wurden, T.P. Intrator, J. Sears, T. Weber, W.J. Waganaar, M.H. Frese, S.D. Frese, J.F. Camacho, S.K. Coffey, V. Makhin, N.F. Roderick, D.G. Gale, M. Kostora, A. Lerma, J.L. McCullough, W. Sommars, G.F. Kiuttu, B. Bauer, S.R. Fuelling, R.E. Siemon, A.G. Lynn, P.J. Turchi. **“**Recent magneto-inertial fusion experiments on the field reversed configuration heating” Nucl. Fusion, **53**, 093003, 2013.
16. M.A. Liberman, J.S. De Groot, A. Toor. “Physics of high-density Z-pinch plasmas.” Springer-Verlag, New York, 1999.

17. A.L. Velikovich, J. Davis. “Implosions, Equilibria, and Stability of Rotating, Radiating Z-Pinch Plasmas,” Phys. Plasmas, **2**, 4513 (1995).
18. S.I. Braginski. “Transport processes in a plasma.” In: “Reviews of Plasma Physics” (M. A. Leontovich, Editor). Consultants Bureau, NY, 1965, p. 205.
19. B.A. Trubnikov. “Particle interactions in a fully ionized plasma.” In: “Reviews of Plasma Physics” (M. A. Leontovich, Editor). Consultants Bureau, NY, 1965, p. 105.
20. S. Ichimaru. “Strongly coupled plasmas - high-density classical plasmas and degenerate electron liquid.” Rev. Mod. Phys., **54**, 1017 (1982); S.F. Garanin, S.F. Kuznetsov, W.L. Atchinson et al., “Numerical simulations of thick aluminum wire behavior under megaampere current drive.” 2009 IEEE Pulsed Power Conference, v.1-2, p. 101 (2009); T.J. Awe, B.S. Bauer, S. Fuelling, et al, “Threshold for Thermal Ionization of an Aluminum Surface by Pulsed Megagauss Magnetic Field.” PRL, **104**, 035001 (2010).
21. R.F. Post, “The magnetic mirror approach to fusion,” Nucl. Fusion **27**, 1579 (1987); D.D. Ryutov, "Open-ended traps," Sov. Phys. Uspekhi **31**, 300 (1988).
22. J.F. Luciani, P. Mora, J. Virmont. “Nonlocal Heat Transport Due to Steep Temperature Gradients.” Phys. Rev. Lett., **51**, 1664 (1983)
23. M. Day, B. Merriman, F. Nadjmabadi, R.W. Conn. “The effect of heat flux limiting on divertor fluid models.” Contrib. Plasma Phys. **36**, 419 (1996).
24. H. Brysk. “Fusion Neutron Energies and Spectra.” Plasma Physics, **15**, 611 (1973).
25. D. B. Henderson, “Burn conditions of marginal Deuterium-Tritium microspheres.” Phys. Rev. Lett. **33**, 1142 (1974).
26. Yu. V. Vasil’ev, D.D. Ryutov. “High-energy part of ion distribution function in a multi-mirror magnetic trap.” Journ. of Appl. Mech. and Techn. Phys, **18**, 295 (1977). Available at: http://link.springer.com/article/10.1007/BF00851646
27. A. G. Petschek and D. B. Henderson, Nucl. Fusion **19**, 1678 (1979).
28. K. Molvig, N. M. Hoffman, B.J. Albright et al. “Knudsen Layer Reduction of Fusion Reactivity.” Phys. Rev. Lett., **109**, 095001 (2012);
29. A. El Nadi, M.N. Rosenbluth. “Infinite β-limit of the drift instability,” Phys. Fluids, **16**, 2036, 1973.
30. D.D. Ryutov. “On Drift Instabilities in Magnetized Target Fusion Devices.” *Physics of Plasmas*, **9**, 4085 (2002). D.D. Ryutov, D. Barnes, B. Bauer, J.H. Hammer, C.W. Hartman, R.C. Kirkpatrick, I.R. Lindemuth, V. Makhin, P. B. Parks, D.B. Reisman, P.T. Sheehey, R.E. Siemon. “Particle and Heat Transport in a Dense Wall-Confined MTF Plasma (Theory and Simulations)”. *Nuclear Fusion*, **43**, 955 (2003).
31. C.A. Jennings, M.E. Cuneo, E.M. Waisman, E. M. et al. “Simulations of the implosion and stagnation of compact wire arrays.” Phys. Plasmas, **17**, 092703 (2010).
32. S. V. Lebedev, A. Ciardi, D. J. Ampleford, S. N. Bland, S. C. Bott, J. P. Chittenden, G. N. Hall, J. Rapley, C. Jennings, M. Sherlock, A. Frank, E. G. Blackman. “Production of radiatively cooled hypersonic plasma jets and links to astrophysical jets.” Plasma Phys. Control. Fusion, **47**, B465–B479 (2005).
33. R.L. Berger, J.R. Albritton, C.J. Randall, E.A. Williams, W.L. Kruer, A.B. Langdon, C.J. Hanna. “Stopping and thermalization of interpenetrating plasma streams” Phys. Fluids, **B3**, 3 (1991).
34. A.V. Gordeev, A.S. Kingsep, L.I. Rudakov. “Electron Magnetohydrodynamics,” Phys. Reports, **243**, 215-315, 1994.

35. L.D. Landau and E.M. Lifshitz. *"Electrodynamics of continuous media."* Pergamon, NY, 1984.
36. P.-A. Gourdain, C.E. Seyler, C. E. "Impact of the Hall Effect on High-Energy-Density Plasma Jets ." Phys. Rev. Lett, **110**, 015002 (2013).
37. P.-A. Gourdain and C. E. Seyler. "Modeling of strongly collimated jets produced by high energy density plasmas on COBRA." Plasma Phys. Contr. Fusion, **56**, 035002 (2014).
38. L. Biermann. "Über den upsprung der Magnetfelder auf Sternen und im Interstellaren Raum." Zeitschrift für Naturforschung, Section A-A, **5**, 65-71, 1950.
39. R.M. Kulsrud, R.Y. Cen, J.P. Ostriker, et al. "The protogalactic origin for cosmic magnetic fields" Astrophys. J., **480** , 481-491 (1997).
40. S.A. Slutz, R.A. Vesey. "High gain inertial fusion." Phys. Rev. Lett., **108**, 025003 (2012).
41. A. B. Sefkow, S. A. Slutz, J. M. Koning, M. M. Marinak, K. J. Peterson, D. B. Sinars, and R. A. Vesey. "Design of magnetized liner inertial fusion experiments using the Z facility" Phys. Plasmas, **21**, 072711 (2014).
42. D.D. Ryutov. "Rayleigh-Taylor Instability in a Finely Structured Medium". Physics of Plasmas, v.3, 4336 (1996).
43. M.A.Dorf. "Viscosity of a multispecies plasma containing hydrogen and high-Z ions" arXiv:1408.3677 [physics.plasm-ph], August 2014.
44. C.J. Hansen, S.D. Kawaler, V. Trimble. *Stellar Interiors*. Springer, 2004.
45. E.N. Parker. "Sweet's mechanism for merging magnetic fields in conducting fluids." J. Geophys. Res., **62** 509 (1957)
46. J.W. Dungey. "Cosmic Electrodynamics." Cambridge University Press, London, 1958.
47. M. Yamada, R. Kulsrud, H. Ji. Rev. Mod. Phys. **82**, 603-664, 2010.
48. N. F. Loureiro, A. A. Schekochihin, S. C. Cowley. "Instability of current sheets and formation of plasmoid chains." Phys. Plas., **14**, 100703 (2007).
49. G. Lapenta Self-Feeding Turbulent Magnetic Reconnection on Macroscopic Scales. Phys. Rev. Lett., **100**, 235001 (2008).
50. A. Bhattacharjee, Yi-Min Huang, H. Yang, and B. Rogers, "Fast reconnection in high-Lundquist-number plasmas due to the plasmoid Instability." Phys. Plasmas, **16**, 112102 (2009).
51. M. Tuszewski. "Field-reversed configuations." Nucl. Fusion, **28**, 2033 (1988).
52. D.C. Barnes, C.E. Seyler, D.V. Anderson. "On compact toruses and energetic particle injection." Proc. 1st US-Japan Joint Symp., Princeton, NJ, 1970.
53. D.L.Book. "NRL Plasma Formulary." *Naval Research Laboratory* (1987).
54. A. B. Mikhailovskii, *"Electromagnetic Instabilities in an Inhomogeneous Plasma."* Institute of Physics, Bristol, 1992.
55. G.E. Vekshtein, D.D. Ryutov, M.D.Spektor, P.Z.Chebotaev. "Nonmagnetic containment of a dense plasma". Applied Mechanics and Technical Physics, No 6, p.3 (1974); available at: http://link.springer.com/article/10.1007/BF00864590
56. G.E.Vekshtein, D.D. Ryutov, P.Z.Chebotaev. "Diffusion of heavy impurities in a dense, wall-confined plasma". Sov. J. Plasma Phys., **1**, p. 220 (1975).
57. L.A. Bol'shov, Yu.A. Dreizin, A.M. Dykhne. "Spontaneous magnetization of electronic thermal conductivity in a laser plasma." JETP Lett. 19. 168 (1974).
58. N.K. Winsor, D.A. Tidman. "Laser Target Model." Phys. Rev. Lett., **31**, 1044 (1973).
59. L.D. Landau and E.M. Lifshitz. *"Fluid Mechanics,"* Pergamon, NY, 1987.

60. D.D. Ryutov, R. P. Drake, J. Kane, E. Liang, B. A. Remington, and W.M. Wood-Vasey. "Similarity criteria for the laboratory simulation of supernova hydrodynamics." Astrophysical Journal, **518**, 821 (1999).
61. D.D. Ryutov, B.A. Remington, H.F. Robey, R.P. Drake. "Magnetohydrodynamic scaling: from astrophysics to the laboratory," Phys. Plasmas, **8**, 1804 (2001).
62. P-A Gourdain, I. C. Blesener, J. B. Greenly, D. A. Hammer, P. F. Knapp, B. R. Kusse, S. A. Pikuz, T. C. Shelkovenko. "High energy density plasmas generated by radial foil explosions." Plasma Phys. Control. Fusion **52**, 055015 (2010).
63. D. J. Ampleford, S.V. Lebedev, A. Ciardi, S. N. Bland, S. C. Bott, G. N. Hall, N. Naz, C. A. Jennings, M. Sherlock, J. P. Chittenden, J. B. A. Palmer, A. Frank, E. Blackman - "Supersonic Radiatively Cooled Rotating Flows and Jets in the Laboratory", Phys. Rev. Letters, **100**, 035001 (2008).
64. D. J. Ampleford, C. A. Jennings, G. N. Hall, S. V. Lebedev, S. N. Bland, S. C. Bott, F. Suzuki-Vidal, J. B. A. Palmer, J. P. Chittenden, M. E. Cuneo, A. Frank, E. G. Blackman, A. Ciardi "Bow shocks in ablated plasma streams for nested wire array z-pinches: A laboratory astrophysics testbed for radiatively cooled shocks." Phys. Plasmas, **17**, 056315 (2010).
65. F. Beg, A. Ciardi, I. Ross, Y. Zhu, A.E. Dangor, K. Krushelnik. "Jet formation and current transfer in X-pinches." IEEE Trans. Plsma Sci., **34**, 2325 (2006).
66. D.M. Haas, S.C. Bott, J. Kim, D.A. Mariscal, R.E. Madden, Y. Eshaq, U. Ueda, G. Collins IV, K. Gunasekera, F.N. Beg, J.P. Chittenden, N. Niasse, C.A. Jennings. "Supersonic jet formation and propagation in x-pinches." Astrophys Space Sci, **336**, 33 (2011).
67. D. Martinez, R. Presura, S. Wright, C. Plechaty, S. Neff, L. Wanex, D.J. Ampleford. "Generation of shear flow in conical wire arrays with a center wire," Astrophys Space Sci, **322**, 205-208 (2009).
68. J. Lacina. "Similarity rules in plasma physics." Plasma Phys. **13**, 303 (1971).
69. B. B. Kadomtsev, "Tokamaks and analysis of scaling." Sov. J. Plasma Phys. **1**, 296 (1975).
70. J. W. Connor and J. B. Taylor. "Scaling laws for plasma confinement." Nucl. Fusion **17**, 1047 (1977).
71. H. Dreicer. "Electron and ion runaway in a fully ionized gas.1." Phys. Rev. **115** , 238-249, 1959; "Electron and ion runaway in a fully ionized gas.2." Phys. Rev. Volume: **117**, 329-342, 1960.
72. M.G. Haines. "Ion beam formation in an *m*=0 unstable Z pinch." Nucl. Instruments and Methods, **207**, 179-185 (1983).
73. R. Deutsch, W. Kies. "Manifestation of an ion acceleration mechanism in computer simulations and plasma-focus experiments." Plasma Physics and Controlled Fusion, **30**, 921-934 (1988)
74. B.A. Trubnikov. "A new hypothesis of cosmic ray generation in plasma pinches." IEEE Trans. Plasma Science, **20**, 898 (1992).
75. V.V. Vikhrev, V.D. Korolev, "Neutron Generation from Z-Pinches" Plasma Physics Reports, **33**, 356–380 (2007).
76. D. Klir, P. Kubes, K. Rezac, J. Cikhardt, J. Kravarik, O. Sila, A. V. Shishlov, B. M. Kovalchuk, N. A. Ratakhin, V. A. Kokshenev, A. Yu. Labetsky, R. K. Cherdizov, F. I. Fursov, N. E. Kurmaev, G. N. Dudkin, B. A. Nechaev, V. N. Padalko, H. Orcikova, K. Turek. "Efficient Neutron Production from a Novel Configuration of Deuterium Gas-Puff Z-Pinch." PRL 112, 095001 (2014) PHYSICAL REVIEW LETTERS
77. F. Suzuki-Vidal, S. Patankar, S. V. Lebedev, S. N. Bland, H. Doyle, D. Bigourd, G. Burdiak,

P. de Grouchy, G. N. Hall, A. J. Harvey-Thompson, E. Khoory, L. Pickworth, J. Skidmore, R.A. Smith and G. F. Swadling. “Observation of energetic protons trapped in laboratory magnetic-tower jets.” New Journal of Physics **15**, 125008 (2013).
78. A. Schmidt, V. Tang, and D. Welch. “Fully Kinetic Simulations of Dense Plasma Focus Z-Pinch Devices.” PRL **109**, 205003 (2012).

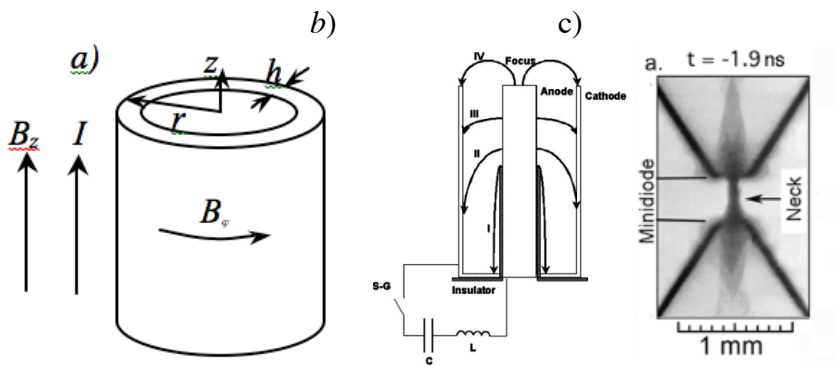

Fig. 1 The geometry of typical Z-pinch configurations: a) Imploding thin-wall liner; the current flows along the axis and creates an azimuthal magnetic field; the $\boldsymbol{j}\times\boldsymbol{B}$ force pushes the liner inward, causing its eventual on-axis collapse; if the liner in the initial state is filled with a pre-formed plasma, it may heat and compress it on axis; to ensure a good thermal insulation of the liner from the walls, an axial magnetic field can be imposed. Instead of a continuous liner, one can use a set of many thin wires stretched along the axis. b) Plasma focus (courtesy L Soto et al, Brazilian J. Phys., **34**, 1814, 2004); the plasma shell passes the stages from I to IV and then implodes on axis; the azimuthal magnetic field pushes the shell from below in the direction normal to the shell. c) X-pinch (courtesy A. Shelkovenko et al, IEEE Transactions on Plasma Science, **42**, 748, 2014); very high current densities can be achieved in the crossing point of two wires at a modest value of the total current.

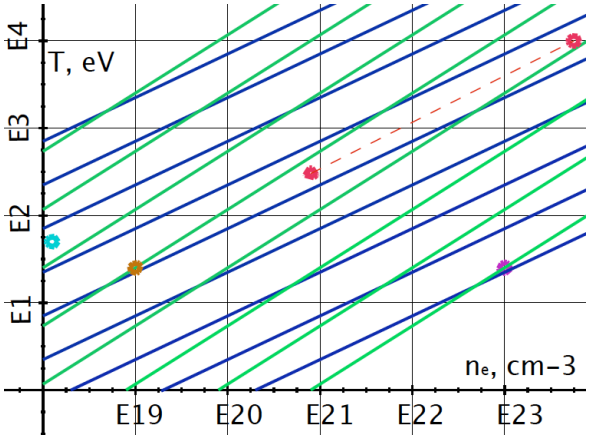

Fig. 2 Characterization of particle collisions: Blue lines represent the constant values of mean-free-paths on the (n_e, T) plane. For the lowest curve the value of the parameters $\lambda_{ei}Z$ for the electrons and $\lambda_{ii}Z^3$ for the ions, is 10^{-8} cm. For every next blue curve this number increases by a factor of 10, reaching 1 cm for the upper-most curve. Green lines represent the lines of constant *e-i* energy-exchange time (Eq. (4)). The lowest green curve corresponds to the value of the parameter $\tau_{ei}^{(E)}(ns)Z/A = 10^{-4}$. For every next curve it increases by a factor of 10, reaching 1000 at the uppermost green curve. Red points roughly correspond to the initial and final parameters of the core DT plasma in MagLIF (Z=1, A=2.5); the system evolves along a dashed line; mean-free path stays below 10 μm. Equilibration time remains less than 1ns during the whole implosion process. The magenta, brown and light-blue points correspond to the plasma parameters in the lines 3, 4 and 5 in Table 1, respectively. When evaluating the mean-free paths and equilibration times for these plasmas mind the presence on the A- and Z-dependent factors in the corresponding expressions. E.g., when evaluating an equilibration time for the brown dot (a carbon plasma), multiply 1 ns by a factor of Z/A=2.

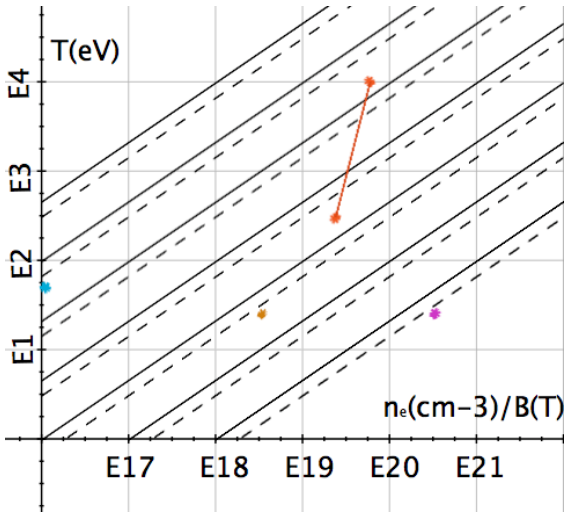

Fig.3. Plasma magnetization. Solid lines describe electrons, dashed lines describe ions. The lines correspond to a constant value of the parameter $ZMag_e$ for the electrons (solid lines) and $Z^2\sqrt{A}Mag_i$ for the ions (dashed lines). At the lowest line for the electrons $ZMag_e=10^{-2}$, for each next line this parameter increases by a factor of 10, ending at 10^4 for the upper-most electron line. For the lowest ion line we also have $Z^2\sqrt{A}Mag_i=10^{-4}$, with a factor of 10 increase to every next line. To find magnetization for some values of T and n_e, one has to choose the line nearest to the corresponding point on the (n_e, T) plane; then, substituting information regarding the ion species one finds the magnetizations $Mag_{e,i}$ for the corresponding point. If the electron and ion temperatures are different, one has to use an appropriate temperature for each plot.

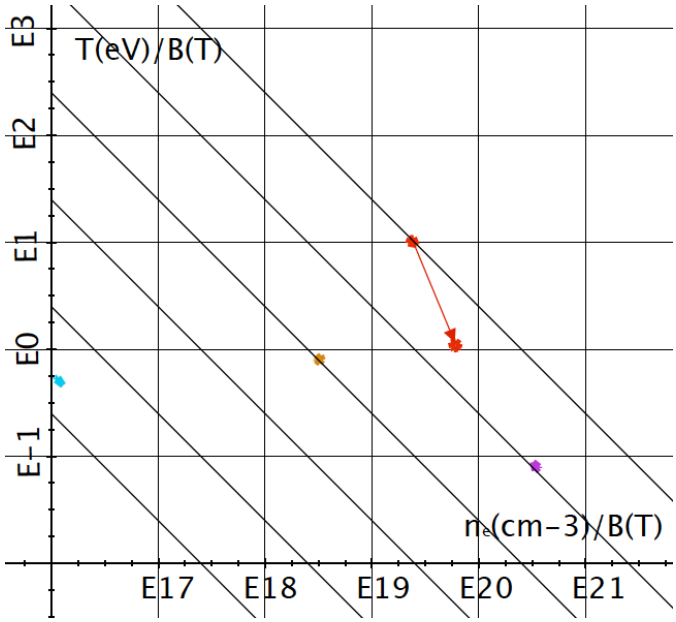

Fig. 4 Parameter β (Eq. (7)). The lines correspond to the constant values of the parameter $\beta Z/(Z+1)$. For the lowest line $\beta Z/(Z+1)=0.001$, for each next line this parameter increases by a factor of 10, ending up at 100 for the upper-most line. The core plasma in the initial state of the MagLIF experiment is shown by the upper red dot, the arrow shows an evolution to the final state. Other dots correspond to the lower three lines in Table 1: magenta to line 3, brown to line 4 and light blue to line 5.

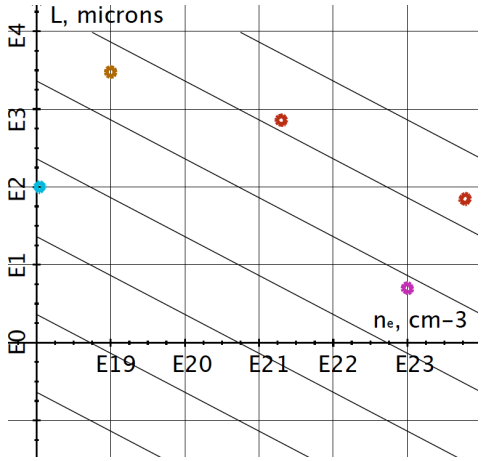

Fig.5. Characterization of the Hall effect in the (n_e, L) plane. The lines correspond to constant values of parameter $Ha\sqrt{Z/A}$. The lowest line corresponds to $Ha\sqrt{Z/A}=1000$, for every higher line it decreases by a factor of 10, ending with 10^{-3} for the upper-most line. The parameter L is a cross-field length scale of the magnetic field variation. Identifying L with the hot plasma radius in the MagLIF concept, and taking the corresponding numbers from lines 1 and 2 of Table 1, we find that the Hall number Ha remains below 10^{-2} during the whole implosion. In other words, the Hall MHD is not affecting the core plasma behaviour in MagLIF. In some astrophysics-related experiments, the Hall effect can be substantial: for the light-blue dot (line 5 in Table 1) the Hall number is ~ 2.

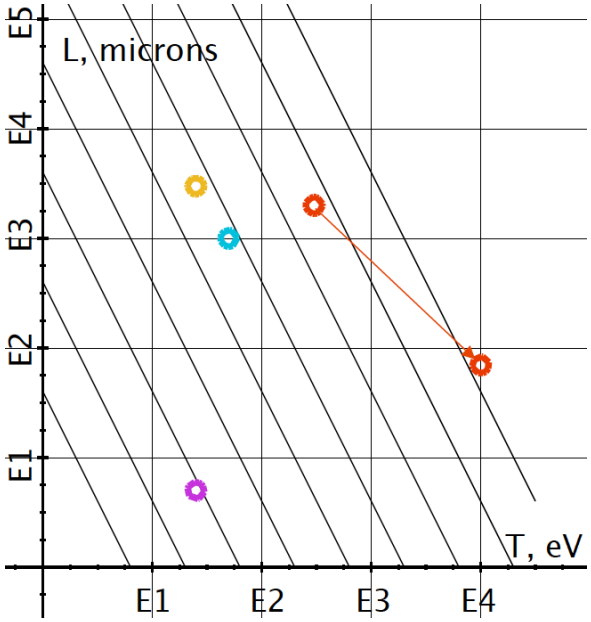

Fig. 6 The Magnetic Reynolds number $\mathrm{Re_M}$ in the (T, L) plane (L is in microns). The lines correspond to constant values of the parameter $\mathrm{Re}_M \sqrt{Z+1} / MZ\sqrt{A}$. The lowest line corresponds to $\mathrm{Re}_M \sqrt{Z+1} / MZ\sqrt{A}$ =0.01; for each next line it increases by a factor of 10, with the upper line corresponding to 10^6. The red dots correspond to the initial and final states of the MagLIF experiment. Mind the presence of the Mach number M in the parametrization of the lines. The magenta, brown and light-blue dots correspond to the 3rd , 4th and 5th lines in Table 1.

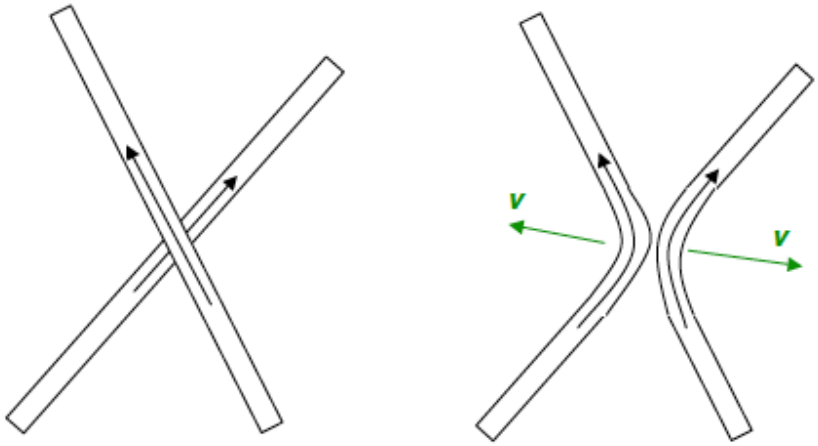

Fig. 7. Magnetic reconnection in two flux tubes. At the left, two flux tubes with an axial magnetic field frozen into each of them are separated by some distance in the direction normal to the figure. They are held in a radial equilibrium by an excess of the thermal pressure outside the flux tubes (a situation that may take place in the solar convective zone). When a slow motion of an external medium brings them close to each other, reconnection may occur near the intersection point; this leads to a release of not only the magnetic energy in the reconnection zone, but also the energy related to the straightening of the flux tubes (the motion indicated by green arrows).

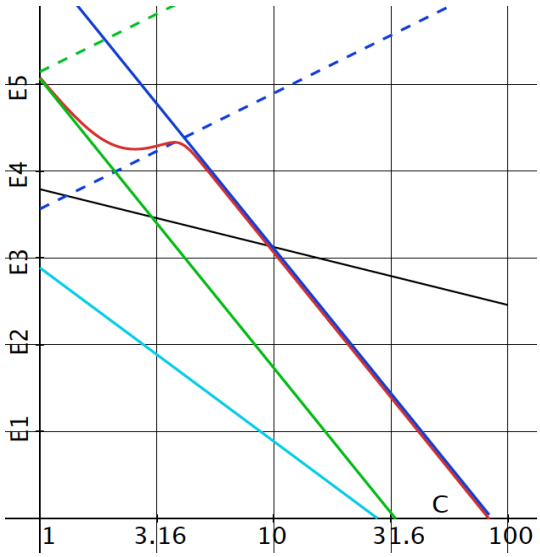

Fig. 8 Transport coefficients for the reference case (Eq. (40)), in cm^2/s. Blue solid line: magnetized ion thermal diffusivity (Ref. 18, Eq. 2.16; Eq. A10) blue dashed line: parallel (un-magnetized) ion thermal diffusivity (Ref. 18, Eq. 2.15, Eq. A9); green solid line: magnetized electron thermal diffusivity (Ref. 18, Eq. 2.13, Eq. A11); red line: total cross-field diffusivity; black line: Bohm diffusivity. For the reference case (Eq. 40), the Bohm diffusivity becomes higher than the classical diffusivity at C=10.

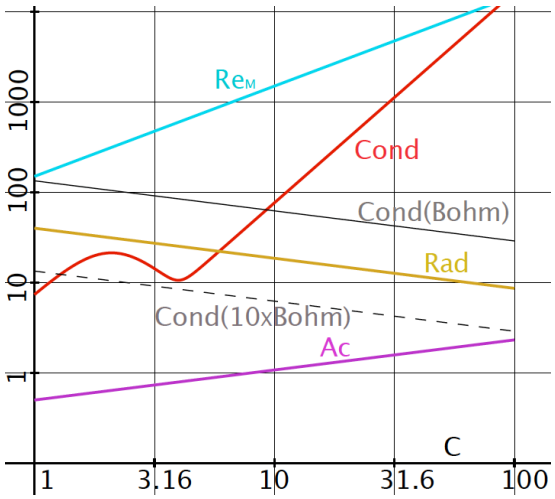

Fig. 9. Dimensionless factors *Cond* (Eq. 50, red line); Re_M (Eq. 51, light blue), *Ac* (Eq. 53, magenta), and *Rad* (Eq. 55, brown) characterizing the quality of the plasma confinement. For reference, we present also the *Cond* plots for $\chi_\perp = \chi_{Bohm}$ (solid black) and $\chi_\perp = 10\chi_{Bohm}$ (dashed black). For the latter case, the anomalous heat conduction starts effecting plasma confinement by the end of implosion.